

OPEN ACCESS

EDITED BY Prahalada Rao, Virginia Tech, United States

REVIEWED BY
Yuanbin Wang,
Northwestern Polytechnical University,
China
Aniruddha Gaikwad,
Machine Learning Researcher,
United States

RECEIVED 01 August 2023 ACCEPTED 06 December 2023 PUBLISHED 21 December 2023

CITATION

Balhara H, Karthikeyan A, Hanchate A, Nakkina TG and Bukkapatnam STS (2023), Imaging systems and techniques for fusion-based metal additive manufacturing: a review.

Front. Manuf. Technol. 3:1271190.
doi: 10.3389/fmtec.2023.1271190

COPYRIGHT

© 2023 Balhara, Karthikeyan, Hanchate, Nakkina and Bukkapatnam. This is an open-access article distributed under the terms of the Creative Commons Attribution License (CC BY). The use, distribution or reproduction in other forums is permitted, provided the original author(s) and the copyright owner(s) are credited and that the original publication in this journal is cited, in accordance with accepted academic practice. No use, distribution or reproduction is permitted which does not comply with these terms.

Imaging systems and techniques for fusion-based metal additive manufacturing: a review

Himanshu Balhara, Adithyaa Karthikeyan, Abhishek Hanchate, Tapan Ganatma Nakkina and Satish T. S. Bukkapatnam*

Wm Michael Barnes'64 Department of Industrial and Systems Engineering, Texas A&M University, College Station, TX. United States

This study presents an overview and a few case studies to explicate the transformative power of diverse imaging techniques for smart manufacturing, focusing largely on various in-situ and ex-situ imaging methods for monitoring fusion-based metal additive manufacturing (AM) processes such as directed energy deposition (DED), selective laser melting (SLM), electron beam melting (EBM). In-situ imaging techniques, encompassing high-speed cameras, thermal cameras, and digital cameras, are becoming increasingly affordable, complementary, and are emerging as vital for real-time monitoring, enabling continuous assessment of build quality. For example, high-speed cameras capture dynamic laser-material interaction, swiftly detecting defects, while thermal cameras identify thermal distribution of the melt pool and potential anomalies. The data gathered from in-situ imaging are then utilized to extract pertinent features that facilitate effective control of process parameters, thereby optimizing the AM processes and minimizing defects. On the other hand, ex-situ imaging techniques play a critical role in comprehensive component analysis. Scanning electron microscopy (SEM), optical microscopy, and 3D-profilometry enable detailed characterization of microstructural features, surface roughness, porosity, and dimensional accuracy. Employing a battery of Artificial Intelligence (AI) algorithms, information from diverse imaging and other multimodal data sources can be fused, and thereby achieve a more comprehensive understanding of a manufacturing process. This integration enables informed decision-making for process optimization and quality assurance, as Al algorithms analyze the combined data to extract relevant insights and patterns. Ultimately, the power of imaging in additive manufacturing lies in its ability to deliver real-time monitoring, precise control, and comprehensive analysis, empowering manufacturers to achieve supreme levels of precision, reliability, and productivity in the production of components.

KEYWORDS

fusion-based metal additive manufacturing, high speed imaging, thermal imaging, optical imaging, vibration-based imaging

1 Introduction

The emergence of Industry 4.0 over the last decade has seen manufacturing industries transforming themselves by integrating physical production and operations with smart digital technologies and big data, thereby creating a highly interconnected network of manufacturing devices resulting in efficient and automated production workflows

(Zhong et al., 2017). The increasing use of sensor-fusion based technologies in manufacturing, wherein data from multiple sensors are fused to produce reliable information, yields a more robust understanding of the physics behind manufacturing processes and significantly contributes towards improving product quality control (Kumar and Garg, 2004). Imaging techniques have emerged as central tools within the space of additive manufacturing, revolutionizing industry.

The machine vision market, which encompasses imaging systems in manufacturing, has been experiencing significant growth. According to a report by Fortune Business Insights (The global machine vision market, 2023), the global machine vision market was valued at around \$9.01 billion in 2022 and is projected to reach \$16.82 billion by 2030, with a compound annual growth rate (CAGR) of 8.2% during the forecast period. The integration of AI and machine learning techniques with imaging systems has further fueled the growth by enabling automated decision-making and real-time monitoring, enhancing overall manufacturing efficiency. From machine vision systems that perform automated quality inspections to thermal imaging cameras that detect anomalies in temperature distributions, imaging technologies are a powerful tool to visualize and understand complex manufacturing processes with unique clarity.

1.1 Imaging techniques

1.1.1 *In-situ* imaging

In the realm of additive manufacturing, two major imaging techniques exist: *in-situ* imaging and *ex-situ* or post-processing imaging. Each technique possesses distinct advantages and disadvantages, but *in-situ* imaging holds significant importance, particularly in the context of real time process monitoring. *In-situ* imaging, within the realm of manufacturing and material processing, is a technique that involves the capture and analysis of data directly within the operational environment. This is done without disrupting ongoing processes or necessitating the removal of samples for external examination.

This method allows for the real-time monitoring and analysis of various phenomena, such as alterations in material properties, structural dynamics, and process conditions. These observations provide valuable insights into the underlying mechanisms at work. By studying the process in its natural state, researchers can gain a holistic understanding of the dynamics and behaviors involved. This facilitates the identification of key patterns and trends, as well as potential areas for optimization or intervention. This technique enables the continuous monitoring of manufacturing processes, resulting in the generation of large volumes of data. Subsequently, these data sets can be subjected to analysis, aiming to extract meaningful and valuable information.

1.1.2 Ex-situ imaging

While not real-time, *ex-situ* imaging techniques offer detailed characterization of the manufactured part. Typically, these techniques involve capturing images and relevant data from samples to analyze their mechanical and structural properties. Notable examples include technologies such as scanning electron microscopy, optical microscopy, and profilometer-based scanning.

These techniques provide highly accurate and precise characterizations of the samples, making them indispensable for quality control as well as research and development efforts.

Ex-situ imaging has been a mainstay in the industry for decades. However, several compelling reasons have underscored the need for *in-situ* imaging techniques. Firstly, *ex-situ* techniques do not provide immediate feedback or the ability to address issues as they arise. This is particularly true for time-sensitive industries such as additive manufacturing, where near real-time adjustments are necessary. Another limitation of *ex-situ* techniques is their inability to capture the process dynamics as the manufacturing process progresses.

In contrast, *in-situ* techniques can circumvent some of the redundancies inherent in *ex-situ* imaging, making them more practical in today's smart additive manufacturing environment. This paper discusses *ex-situ* imaging techniques tangentially, with a specific focus on the integration of AI and ML frameworks.

The utilization of these *in-situ* imaging approaches offers a data-driven perspective, allowing for the identification of patterns, anomalies, and correlations that might remain unnoticed using conventional methods (Iquebal et al., 2020). The continuous monitoring and analysis of data streams enable real-time decision-making, as deviations from desired process conditions or quality specifications can be promptly identified. This timely feedback loop allows for immediate adjustments and interventions to uphold or improve manufacturing performance. However, these *in-situ* image techniques are prevented in implementation due to high markup prices, which over the time will become feasible for everyone to use such techniques.

1.2 Techno-economic barriers and opportunities

While the initial high costs currently deter the widespread adoption of *in-situ* imaging techniques, ongoing research and technological advancements are anticipated to lead to cost reductions. As these costs decrease, these techniques will become increasingly accessible to a wider range of manufacturers, enabling them to harness the advantages of data-driven decision-making, real-time monitoring, and process optimization. The industry also faces significant challenges, such as the effective development and deployment of an appropriate edge computing setup capable of analyzing large volumes of high-quality image data in real-time. This capability to process vast amounts of data within milliseconds is crucial for applications where prompt decision-making is essential.

At present, the options for edge computing are limited, either due to high capital investment or processing speeds. However, with advancements in GPU technologies, the development of more powerful and energy-efficient hardware, and better-optimized algorithms, it has become feasible to achieve near real-time decision-making, even in implementations where all raw data is used for analysis. On another front, there has been a shift towards the concept of 'just-the-right data' or feature extraction. In this approach, only the important features of the raw data are extracted, while the redundant imaging data is discarded, enabling real-time *in-situ* monitoring.

TABLE 1 Imaging techniques used in different fusion-based additive manufacturing processes.

Aspects	AM process	lmaging technique	Sensor	Feature	Spatial and temporal resolution
Geometry	SLM (Black et al., 2023)	Optical	CCD	Material flow and densification	60 μm/pixel, 75 Hz
	SLM (Abhilash and Ahmed, 2023)	Optical	USB digital camera	Corner/Edge dimensions	-
	SLM (Xie et al., 2022)	Optical	-	Linear zone boundaries	1,080 × 1920 pixels*, 2,158 fps
	SLM (Lapointe et al., 2022)	Optical	Photodiode	Thins walls and overhangs	40 kHz
	SLM (Özsoy et al., 2021)	Optical	CMOS	Layer width	5.4 μm/pixel
	SLM (Zhang et al., 2023a)	Optical	3D scanner	Deviations of common geometric features (right angles, acute angles, arcs, rings, etc.) and warpage	5.4 μm/pixel, 42 fps
	DED (Regulin and Barucci, 2023)	Optical	In-process depth meter (IDM), CMOS	Build height	30 FPS
	Wire-DED (Xiong et al., 2016)	Optical	Passive vision sensor, CCD	Layer width	Wavelength of 650 nm
	Wire-DED (Becker et al., 2021)	Optical	OCT	Track height	Wavelength of 1,550 nm, 20 kHz
	Wire-DED (Li et al., 2021b)	Optical	SLS	Bead height and width	-
	Wire-DED (Radel et al., 2019)	Optical	Camera	Deposit radius	30 μm/pixel
	SLM (Liu et al., 2022)	Thermography	LWIR sensor	Layer thickness	325 μm/pixel, 200 Hz
	Wire-DED (Bernauer et al., 2022a)	Thermography	Pyrometer	Bead width	1.45–1.65 μm/pixel, 1 kHz
	EBM (Renner et al., 2022)	Electron optical imaging	Backscattered Electron	Bulging	53.3 µm/pixel, 32 MHz
	EBM (Arnold and Körner, 2021)	Electron optical imaging	Backscattered Electron	Dimensional accuracy	47 μm/pixel, 1.8 s
	EBM (Wong, 2020)	Electron optical imaging	Backscattered Electron	Surface tilt	100 μm/pixel, 27.3 s
Morphology	SLM (Cherif et al., 2023)	High speed optical	CMOS	Balling, irregularity, overheating	1,022 × 428 pixels*, 2000 FPS
	SLM (Chebil et al., 2023)	High speed optical	CMOS	Spatter	80 μm/pixel, 10kfps
	SLM (Boschetto et al., 2023)	Optical	CCD	Lack-of-fusion porosity, geometrical deformations	1,280 × 1,024 pixels*
	SLM (Bugatti and Colosimo, 2022)	Optical	CMOS	Hot spots	121 × 71 pixels*, 300 FPS
	SLM (Boschetto et al., 2022)	Optical	CCD	Voids, lack of powder	1,280 × 1,024 pixels*
	SLM (Vallabh et al., 2021)	Optical high speed	CMOS	Spatter	0.5 μm/pixel, 1000 FPS
	SLM (Zhang et al., 2023b)	High speed optical	CMOS	Thickness, balling	35.56 μm/pixel
	SLM (Lu et al., 2020)	Optical	Photo interrupter	Porosity, lack of fusion defects	10-13 μm/pixel
	SLM (Yan et al., 2022)	High speed optical	CMOS	Hot spots	126 × 136 pixels*, 150 fps
	SLM (Lin et al., 2022)	Optical high speed	CMOS	Spatter	8 μm/pixel, 2 kHz
	SLM (Jiang et al., 2023)	Optical	CMOS	Balling, crack, debris, lack of powder	80 μm/pixel, 6 fps
	SLM (Fischer et al., 2021)	Optical	CMOS	Balling, spatters, surface porosity	24 μm/pixel
	SLM (Yang et al., 2021)	Optical and Thermography	Coaxial camera, pyrometer	Metrology-roughness, density of part	160 × 160 pixels*, 2.5 kHz
	DED (Yang et al., 2023)	High speed optical	CMOS	Spatter and plume	7 × 5 mm ² , 5,000 fps
	DED (Mi et al., 2023)	High speed optical	CMOS	Spatter	1,280 × 896 pixel*, 30,000 fps
	DED (Sun et al., 2020)	Optical high speed	CMOS	Melt pool	100 fps
	DED (Min et al., 2022)	High speed optical	CMOS	Surface dust	1,280 × 896 pixels, 30,000 fps
	DED (Chen et al., 2020)	Optical	CCD	Melt pool width	-
	EBM (Grasso, 2021)	Optical	CMOS	Inhomogeneity and irregularities	130 μm/pixel
	DED (Reich et al., 2022)	Optical-Laser	2D, 3D triangulation scanners	Surface deformation	12 μm, 300 Hz
	EBM (el Farsy et al., 2023)	Laser spectroscopy	Diode laser	Plume	1 MHz
	SLM (Guerra et al., 2022)	Optical coherence tomography	NIR, LWIR, CMOS	Porosity, lack of fusion and Geometric distortions	26 μm/pixel
	SLM (O'Dowd et al., 2021)	Interferometry	Projector and camera	Keyhole and lack of fusion porosity	50 μm/pixel
	DED (Ma et al., 2023)	Interferometry	Coherent optical sensor	Keyhole porosity	1,000 Hz

(Continued on following page)

TABLE 1 (Continued) Imaging techniques used in different fusion-based additive manufacturing processes.

DED (Millon et al., 2018) Laser Ultrasonic Imaging SLM (Raffestin et al., 2023) Ultrasonic Imaging Ultrasonic Transducer SLM (Alliam et al., 2023) Phased array Ultrasonic Testing Ultrasonic Transducer Lack of fusion pores 12.5 MHz, spatial resolution 0.5 to Ultrasonic Imaging SLM (Davis et al., 2019) Laser Ultrasonic Imaging Two-wave mixing interferometer Lack of fusion pores Lack of fusion pores Lack of fusion pores 12.5 MHz, spatial resolution 0.5 to SLM (Davis et al., 2021) Phased array Ultrasonic Testing Two-wave mixing interferometer Lack of fusion pores 6.3 µm Laser Ultrasonic Imaging SLM (Homarvar et al., 2021) Phased array Ultrasonic Testing Ultrasonic Transducer Internal defects 0.132 mm at 50 MHz Ultrasonic Transducer Lack of fusion pores 6.3 µm Internal defects 0.132 mm at 50 MHz Internal defects 0.132 mm at 50 MHz Ultrasonic Transducer Lack of fusion pores 6.3 µm Internal defects 0.132 mm at 50 MHz Ultrasonic Transducer Internal defects 0.132 mm at 50 MHz Ultrasonic Transducer Lack of fusion pores 6.3 µm 10.112 mm at 50 MHz Ultrasonic Transducer Internal defects 0.132 mm at 50 MHz Ultrasonic Transducer Internal defects 0.132 mm at 50 MHz Internal defects 0.132 mm at 50 MHz Ultrasonic Transducer Internal defects 0.132 mm at 50 MHz Ultrasonic Transducer Internal defects 0.132 mm at 50 MHz Internal defects 1.042 mm at 50 MHz	Aspects	AM process	lmaging technique	Sensor	Feature	Spatial and temporal resolution
DID (Obsert and A. 2021) Thermography Did (State and Economic State) Did (State and Economi		DED (Su et al., 2023)	Thermography	IR sensor	Surface roughness, porosity	1,064 nm, 64 × 48 pixels
DIFF Calhor and Kenevore. DIFF Calhor and A. 2023) The managedy: DIFF cannot are seen and a company of the secondary of the		DED (Liao et al., 2022)	Thermography	IR sensor	Melt pool depth	200 μm, 25 Hz
Diff Colors of a 2023 Thereography The secondary presenter imaging Molt peal temperature 11 jumples 4, 25 life		DED (D'Accardi et al., 2023)	Thermography	IR sensor	Residual melted powder	0.5 mm/pixel, 100 Hz
DED (See et al. 2022) Thermography Bit sensor Melt pool size 65 cold profes 1 Melt pool size 65 cold profes 2 pool pool pool profes 65 cold profes 2 pool pool pool profes 65 cold profes 2 pool pool pool pool pool pool pool po			Thermography	CMOS (Infrared imaging)	Melt pool size	640 × 480 pixels*, 200 fps
DED (All et al. 2022) Thermography Bremore Mit pool size 64 × 64 ptools. 1 bits of 2005 of the Notice of 2005 of 2005 of the Notice		DED (Smoqi et al., 2022)	Thermography	Two-wavelength pyrometer imaging	Melt pool temperature	11 μm/pixel, 2.5 Hz
DED (Ma and Economic, 2008) Wiss-DED (Glasses and A., 2009) Thermography Wiss-DED (Glasses and A., 2009) DED (Glasses and A., 2009) DED (Glasses and A., 2009) Loser Ultrassocic Insigning Larer Interferometer Porce and defects DED (Glasses and 2021) Loser Ultrassocic Insigning Loser Depyder Velocometer DED (Glasses and 2021) Loser Ultrassocic Insigning Loser Depyder Velocometer Lack of fusion porce and defects DED (Glasses and 2021) Loser Ultrassocic Insigning Vero were mitting interferometers Each of fusion porce and defects Detect 13 Mill Animated Response (200 glob- frequency resolutions of 3 Mill Mill (Malmer et al., 2021) Placed army Ultrassocic Transductor Ultrassocic Insigning Ultrassocic Transductor Ultrassocic Insigning Ultrassocic Transductor Ultrassocic Transductor Ultrassocic Insigning Ultrassocic Transductor Ultrassocic Transductor Ultrassocic Insigning Ultrassocic Transductor United State Sta		DED (Su et al., 2022a)	Thermography	IR sensor	Melt pool size	0.5 mm/pixel
Wee DED (General ed., 2010) Lear gradiumter Cancers and lear popicione Person and defense of the pod state Person and defense of the many state (10.0 Miles) Person and defense of the many state (10.0 Miles) DED (State ed., 2012) Lear (Unrossoit Iransphor) Lear (Unrossoit Iransphor) DED (State ed., 2011) Lear (Unrossoit Iransphor) DED (State ed., 2011) Lear (Unrossoit Iransphor) DED (Miles) et al., 2011) Lear (Unrossoit Iransphor) Two save mixing interferenater DED (Miles) et al., 2011) Lear (Unrossoit Iransphor) Two save mixing interferenater DED (Miles) et al., 2011) Lear (Unrossoit Iransphor) Two save mixing interferenater DED (Miles) et al., 2011) Lear (Unrossoit Iransphor) Two save mixing interferenater DED (Miles) et al., 2012) Chrossoit Iransphor Two save mixing interferenater DED (Miles) et al., 2012) Chrossoit Iransphor Trossing Chrossoit Iransphor DED (State ed., 2011) Parts (Generater) and Meephology-designed sovities 10 Miles Miles (Miles) et al., 2012) Parts (Generater) and Meephology-designed sovities 112 Miles Miles (Miles) et al., 2012) Parts (Generater) and Meephology-designed sovities 113 Miles Chrossoit Iransphor Trossing SMM (Decret al., 2011) Spatially Resolved Accounts Section and grave power mixing interferenater DED (Turbolation et al., 2011) Section and grave power mixing interferenater DED (Turbolation et al., 2011) Parts (Generater) and Meephology-designed sovities 113 Miles Lear (Decretos Section Decretos Carlos S		DED (Ali et al., 2022)	Thermography	IR sensor	Melt pool size	64 × 64 pixels*, 1 kHz
Wite DED (Remote et al., 2019) Wite DED (Collows et al., 2019) Thermography Thermol comers, lover line scanner WAMM (Humag et al., 2021) Lover Ultrasonic Imaging DED (Onlow et al., 2021) Lover Ultrasonic Imaging DED (Collows et al., 2021) Lover Ultrasonic Imaging DED (Collows et al., 2021) Liber Ultrasonic Imaging DED (Millson et al., 2021) Liber Ultrasonic Imaging DED (Millson et al., 2021) Liber Ultrasonic Imaging Ultrasonic Transducer Two voere mixing interferometer Lack of fusion north and pass personally frequency resolution of 20 Millson et al., 2021) SMM (Allim et al., 2021) SMM (Allim et al., 2021) Liber Ultrasonic Imaging Ultrasonic Transducer Two voere mixing interferometer Lack of fusion pores and defects Consider were based Ultrasonic Transducer Part's Geometry and Montphology-designed cartiers 10 Mills SMM (Allim et al., 2021) Love Ultrasonic Imaging Ultrasonic Transducer Tacting SMM (Geometri et al., 2021) Lover Ultrasonic Imaging Ultrasonic Transducer Lack of fusion pores and defects Detect 13 Mill surpose and defects Lack of fusion pores and defects Detect 13 Mill surpose and defects Lack of fusion pores and defects Detect 15 Mill surpose and defects Lack of fusion pores and defects Lack of fusion pores and defects Detect 15 Mill surpose and defects Lack of fusion pores and defects Detect 15 Mill surpose and defects Lack of fusion pores and defects Detect 15 Mill surpose and defects Lack of fusion pores and defects Detect 15 Mill surpose and defects Lack of fusion pores and defects Lack of fusion pores and defects Detect 15 Mill surpose and defects Lack of fusion pores and defects Lack of fusion			Thermography	IR sensor	Melt pool area	128 × 128 pixels*
Wire DED (Gibbon et al., 2022) Uranonic Imaging DED (Bake et al., 2022) Laser Uranonic Imaging DED (Bake et al., 2022) DED (Carbon et al., 2022) DES (Carbon et al., 2023) DES (Wire-DED (Gibson et al., 2020)	Thermography	IR sensor	Melt pool size	2,600 to 3,400 pixels*
WAAM (Glange et al., 2022) Laser profeometer Camera and laser projector Bulges, dents, surface poses 1 mm/pixel, 100 like DED (Glade et al., 2022) Laser Ultrasonic Imaging Laser Interferometer Power and defects Power and defects DED (Cacho et al., 2021) DED (Glade et al., 2021) DED (Glade et al., 2021) Ultrasonic Imaging Laser Doppler Vibrometer Lack of fusion and gas processity DED (Gline et al., 2021) DED (Gline et al., 2021) Laser Ultrasonic Imaging Laser Doppler Vibrometer Lack of fusion and gas processity Elected Ultrasonic Imaging DED (Gline et al., 2021) DED (Gline et al., 2021) DED (Gline et al., 2021) Ultrasonic Imaging Laser Doppler Vibrometer Lack of fusion powers and defects SIM (Gline et al., 2022) Defect If Milk advanced freque and Gl Imaging Ultrasonic Transducer Part's Geometry and Morphology-designed certites SIM (Gline et al., 2022) Phased array Ultrasonic Testing Guided waves based Ultrasonic Transducer Lack of fusion powers Lack of fusion powers 12.5 Milks, sprind resolution 0.5 s. SIM (Gline et al., 2022) Defect I Transducer Testing SIM (Gline et al., 2022) Defect I Transducer Testing SIM (Gline et al., 2022) Defect I Transducer Testing SIM (Gline et al., 2023) Defect I Transducer Testing SIM (Gline et al., 2023) Defect I Transducer Testing SIM (Gline et al., 2023) The more mixing interferometer Lack of fusion powers 12.5 Milks, sprind resolution 0.5 s. Ultrasonic Transducer Testing SIM (Gline et al., 2023) The more mixing interferometer Lack of fusion powers 12.5 Milks, sprind resolution 0.5 s. Soffice Defects Surface roughease and solid state phase changes 12.5 Milks, sprind resolution 0.5 s. DED (Grand-Milander et al., 2021) The more power mixing interferometer DED (Grand-Milander et al., 2021) The more power of the			Thermography	Pyrometer	Melt pool temperature	1.45 1.65 μm, 1 kHz
DED (fashes et al., 2022) Laser Ultrasonic Imaging Ultrasonic Transducer DED (Sasdo et al., 2021) DED (Sasdo et al., 2021) Ultrasonic Imaging Ultrasonic Transducer DED (Jase et al., 2023) Laser Ultrasonic Imaging Ultrasonic Transducer DED (Millon et al., 2023) Laser Ultrasonic Imaging Laser Doppler Vibrometer Lack of fauton pores and defects DED (Millon et al., 2023) Laser Ultrasonic Imaging Ultrasonic Transducer SIAM (Millon et al., 2023) Ultrasonic Imaging Ultrasonic Transducer SIAM (Millon et al., 2023) Ultrasonic Imaging Ultrasonic Transducer Part's Geometry and Morphology-designed estities SIAM (Jallin et al., 2023) Phased array Ultrasonic Transducer SIAM (Davis et al., 2023) Phased array Ultrasonic Transducer SIAM (Davis et al., 2023) SIAM (Davis et al., 2021) SIAM (Davis et al., 2021) SIAM (Ultrasonic Imaging Ultrasonic Transducer Testing SIAM (Ultrasonic Imaging SIAM (Ultrasonic Imaging) SIAM (Ultrasonic Imaging SIAM (Ultrasonic Imaging) SIAM (Ultrasonic Imaging SIAM (Ultrasonic Imaging) Two wave mixing interferometer Lack of fusion pores 12.5 Mills. spatial resolution 0.5 s jun SIAM (Ultrasonic Imaging) SIAM (Ultrasonic Imaging) SIAM (Ultrasonic Imaging) SIAM (Ultrasonic Inaging) Two wave mixing interferometer Lack of fusion pores 12.5 Mills. spatial resolution 0.5 s jun SIAM (Ultrasonic Imaging) Two wave mixing interferometer Lack of fusion pores 12.5 Mills. spatial resolution 0.5 s jun SIAM (Ultrasonic Imaging) SIAM (Ultrasonic Imaging) Two wave mixing interferometer Lack of fusion pores 12.5 Mills. spatial resolution 0.5 s jun Jun Microstructure DED (Granbidundar et al., 2014) Spatially Resolve		Wire-DED (Gibson et al., 2019)	Thermography	Thermal camera, laser line scanner	Melt pool size	-
Wire-DED (Chabet et al., 2021) Wire-DED (Soebs et al., 2021) Ultrasonic Imaging Ultrasonic Transducer DED (Line et al., 2023) Laser Ultrasonic Imaging Laser Doppler Vibrometer Lack of fusion and gas personity Ultrasonic reagonase (29 µ)- frequency resolutions of 20 Mile DED (Mallon et al., 2023) Laser Ultrasonic Imaging Two-wave mixing interferometer Lack of fusion porce and defects Detect 13 Mile Stressonal Freque and 0.4 mm are flavor SIM (Faffeste et al., 2022) SIM (Allium et al., 2022) SIM (Allium et al., 2022) Fibrated array Ultrasonic Tenting Two-wave mixing interferometer Lack of fusion porce and defects 10 Mile SIM (Paris et al., 2022) SIM (Desiro et al., 2023) Laser Ultrasonic Imaging Ultrasonic Transducer Tenting SIM (Desiro et al., 2019) Laser Ultrasonic Imaging Two-wave mixing interferometer Lack of fusion porce Lack of fusion porce 12.5 Mile, spatial resolution 0.5 1 SIM (Benis et al., 2019) SIM (Benis et al., 2019) Phased array Ultrasonic Tenting Two-wave mixing interferometer Lack of fusion porce All and fusion porce SIM (Binch et al., 2019) Phased array Ultrasonic Tenting Two-wave mixing interferometer Lack of fusion porce 12.5 Mile, spatial resolution 0.5 1 Lack of fusion porce 12.5 Mile, spatial resolution 0.5 1 Lack of fusion porce 12.5 Mile, spatial resolution 0.5 1 Lack of fusion porce 12.5 Mile, spatial resolution 0.5 1 Lack of fusion porce 12.5 Mile, spatial resolution 0.5 1 Lack of fusion porce 12.5 Mile, spatial resolution 0.5 1 Lack of fusion porce 12.5 Mile, spatial resolution 0.5 1 Lack of fusion porce 12.5 Mile, spatial resolution 0.5 1 Lack of fusion porce 12.5 Mile, spatial resolution 0.5 1 Lack of fusion porce 12.5 Mile, spatial resolution 0.5 1 Lack of fusion porce 12.5 Mile, spatial resolution 0.5 1 Lack of fusion porce 12.5 Mile, spatial resolution 0.5 1 Lack of fusion porce 12.5 Mile, spatial resolution 0.5 1 Lack of fusion porce 12.5 Mile, spatial resolution 0.5 1 Lack of fusion and gas porce 12.5 Mile		WAAM (Huang et al., 2022)	Laser profilometer	Camera and laser projector	Bulges, dents, surface pores	1 mm/pixel, 100 Hz
DED (Sarelo et al., 2021) Ultrasonic Imaging DED (Liu et al., 2023) Laser Ultrasonic Imaging Laser Depoter Variementer Lack of fusion and gas perceity DED (Millon et al., 2018) Laser Ultrasonic Imaging SLM (Raffestin et al., 2018) Laser Ultrasonic Imaging Ultrasonic Transducer SLM (Raffestin et al., 2023) Ultrasonic Imaging Ultrasonic Transducer Part's Geometry and Morphology-designed cavities SLM (Allam et al., 2023) Ultrasonic Imaging Ultrasonic Transducer Ultrasonic Transducer Lack of Fusion defects Cauded waves based Ultrasonic Imaging SLM (Davis et al., 2019) Laser Ultrasonic Imaging SLM (Davis et al., 2019) Laser Ultrasonic Imaging SLM (Davis et al., 2019) Laser Ultrasonic Imaging SLM (Housiver et al., 2011) Phased array Ultrasonic Transducer SLM (Housiver et al., 2011) Spatially Recolved Acoustic Pades Generation Laser, Mask, Detection Later, and Knife Edge Detector Microstructure DED (Farshbalunfar et al., 2017) ShaS and Optical Microscopy Il R sensor Cooling rate, grain structure, microbardness DED (Farshbalunfar et al., 2021) Thermography DED (Carchida et al., 2023) Thermography DED (Carchida et al., 2023) Thermography DED (Carchida et al., 2023) Thermography Thermography Thermal camera Placer Generation Laser, Mask, Detection Cooling rate, grain structure, microbardness S-4 µm/pixel, 30 Hz DED (Carchida et al., 2023) Thermography Thermal camera Place Generation Laser, Mask, Detection Microstructure SLM (Recis et al., 2023) Thermography Thermal camera Place Generation Laser, Mask, Detection Microstructure microbardness S-4 µm/pixel, 50 Hz DED (Carchida et al., 2023) Thermography Thermal camera Place Generation Laser, Mask, Detection Microstructure lunging and Goalo Orientation Sectroscopy SLM (Smith et al., 2014) Spotially Recolved Acoustic Spectroscopy Placed Generation Laser, Mask, Detection Laser, and Knife Edge Detector Microstructure lunging and Goalo Orientation Sectroscopy Placed Generation Laser, Mask, Detection Laser, and Knife Edge Detecto		DED (Bakre et al., 2022)	Laser Ultrasonic Imaging	Laser Interferometer	Pores and defects	
DED (Liu et al., 2023) Laser Ultrasonic Imaging Laser Deppler Vibrometer Lack of fusion and gas perceity frequency resolution of 20 kHz frequency resolu				Ultrasonic Transducer	Pores and defects	-
DED (Millon et al., 2018) Laser Ultrasonic Imaging Two-wave mixing interferometer Lack of fusion pores and defects Deter 18 Hitz ultrasonic frague and 0.1-mm size flavor and 0.1-m		DED (Sotelo et al., 2021)	Ultrasonic Imaging	Ultrasonic Transducer	Surface roughness and solid state phase changes	-
SLM (Raffestin et al., 2023) Ultrasonic Imaging Ultrasonic Transducer SLM (Allum et al., 2022) Phased array Ultrasonic Transducer Ultrasonic Transducer Lack of fusion pores Lack of fusion pores 12.5 MHz, spatial resolution 0.5 to multiplication of fusion pores SLM (Davis et al., 2019) Laser Ultrasonic Imaging Two-wave mixing interferometer Lack of fusion pores 63 µm SLM (Honevar et al., 2021) Phased array Ultrasonic Transducer Ultrasonic Transducer Ultrasonic Transducer Lack of fusion pores 63 µm SLM (Honevar et al., 2021) Phased array Ultrasonic Transducer Ultrasonic Transducer Ultrasonic Transducer Internal defects 0.112 mm at 50 MHz SLM (Hirsch et al., 2018) Spatially Resolved Acoustic Spectroscopy SLM (Hirsch et al., 2017) SRAS and Optical Microstructure DED (Farshidiunfur et al., 2017) DED (Farshidiunfur et al., 2018) DED (Farshidiunfur et al., 2018) DED (Farshidiunfur et al., 2018) Thermography Thermal camera DED (Surface defects Cooling rate, grain structure, microbardness 0.5 mm/pixel, 30 Hz 2016) DED (Chechik et al., 2023) Thermography Thermal camera Phase transformation, grain structure, microbardness 0.5 mm/pixel, 30 Hz DED (Farshidiunfur et al., 2016) Thermography Thermal camera Phase transformation, grain size, melt pool width 0.15 mm/pixel, 1000 FPS Microstructure variations Morphology-Surface and subsurface pores SLM (Smith et al., 2014) Spatially Resolved Acoustic Spectroscopy SLM (Smith et al., 2014) Spatially Resolved Acoustic Spectroscopy Publed Generation Laser, Mask, Detection Laser, and Knife Edge Detector Microstructure variations Morphology-Surface and subsurface pores SLM (Smith et al., 2014) Spatially Resolved Acoustic Spectroscopy Publed Generation Laser, Mask, Detection Laser, and Knife Edge Detector Microstructure Imaging and Grain Orientation Alicrostructure Imaging and Grain Orientation Alicrostructure Imaging and Grain Orientation Alicrostructure Imaging and Grain Orientation		DED (Liu et al., 2023)	Laser Ultrasonic Imaging	Laser Doppler Vibrometer	Lack of fusion and gas porosity	Ultrasonic response (50 µs)– frequency resolution of 20 kHz
SIM (Allam et al., 2022) Phased array Ultrasonic Tensiducer Guided waves based Ultrasonic Imaging SIM (Davis et al., 2019) SIM (Davis et al., 2019) Phased array Ultrasonic Imaging SIM (Honarvar et al., 2021) Phased array Ultrasonic Imaging SIM (Hinch et al., 2011) Phased array Ultrasonic Transducer Ultrasonic Transducer Internal defects SIM (Hinch et al., 2018) Spatially Resolved Acoustic Spectroscopy SIM (Hinch et al., 2017) SRAS and Optical Microstructure DED (Farshidianfar et al., 2014) DED (Farshidianfar et al., 2013) Thermography IR sensor Cooling rate, grain structure, microhardness DED (Farshidianfar et al., 2023) Thermography Thermal camera DED (Farshidianfar et al., 2023) Thermography Thermal camera First agency Thermography Thermal camera Phase transformation, grain size, melt pool width O.5 mm/pixel, 100 FPS SIM (Plirich et al., 2019) SIM (Plirich et al., 2019) SIM (Plirich et al., 2019) SIM (Smith et al., 2014) Spatially Resolved Acoustic Spectroscopy Laser, and Knife Edge Detector Laser, Mask, Detection Laser, and Knife Edge Detector Laser, and Knife Edge Detector All Cooling rate, grain structure, microhardness D.5 mm/pixel, 30 Hz DED (Farshidianfar et al., 2023) Thermography Thermal camera First marea, average hardness SA µm/pixel, 75 FPS DED (Farshidianfar et al., 2016) SEM (Smith et al., 2019) Spatially Resolved Acoustic Spectroscopy Laser, and Knife Edge Detector Laser, Mask, Detection Laser, Mask, Detection Laser, Mask Detection Laser, Mask, Detection Laser, Mask, Detection Laser, Mask, Detection Microstructure variations Morphology-Surface and subsurface pores SIM (Smith et al., 2014) Spatially Resolved Acoustic Spectroscopy Laser, and Knife Edge Detector Microstructure Imaging and Grain Orientation 20 µm		DED (Millon et al., 2018)	Laser Ultrasonic Imaging	Two-wave mixing interferometer	Lack of fusion pores and defects	Detect 15 MHz ultrasound frequency and 0.1-mm size flaws
Testing Guided waves based Laser Doppler Vibrometer Lack of fusion pores 12.5 MHz, spatial resolution 0.5 or		SLM (Raffestin et al., 2023)	Ultrasonic Imaging	Ultrasonic Transducer	Part's Geometry and Morphology-designed cavities	10 MHz
SLM (Davis et al., 2019) Laser Ultrasonic Imaging SLM (Honarvar et al., 2021) Phased array Ultrasonic Testing SLM (Hinsch et al., 2018) Spatially Resolved Acoustic Spectroscopy SLM (Hinsch et al., 2017) SRA and Optical Microstructure DED (Farshidianfar et al., 2018) DED (Su et al., 2023) Thermography Thermal camera DED (Su et al., 2023) Thermography Thermal camera DED (Su et al., 2021) DED (Farshidianfar et al., 2016) Thermography Thermal camera Phase transformation, grain size, melt pool width O.5 mm/pixel, 30 Hz DED (Farshidianfar et al., 2016) Thermography Thermal camera Phase transformation, grain size, melt pool width O.5 mm/pixel SLM (Pieris et al., 2019) Spatially Resolved Acoustic Spectroscopy Pulsed Generation Laser, Mask, Detection Laser, and Knife Edge Detector Cooling rate, grain structure, microhardness O.5 mm/pixel, 30 Hz Cooling rate, grain structure, microhardness O.5 mm/pixel, 30 Hz DED (Su et al., 2023) Thermography Thermal camera Grain area, average hardness 5.4 µm/pixel, 75 FPS DED (Su et al., 2024) Spatially Resolved Acoustic Spectroscopy Results Edge Detector Microstructure variations Morphology-Surface and subsurface pores SLM (Smith et al., 2014) Spatially Resolved Acoustic Spectroscopy Pulsed Generation Laser, Mask, Detection Laser, and Knife Edge Detector Microstructure Imaging and Grain Orientation 20 µm		SLM (Allam et al., 2022)		Ultrasonic Transducer	Lack of Fusion defects	-
SLM (Honarvar et al., 2021) Phased array Ultrasonic Tenting SLM (Hirsch et al., 2018) Spatially Resolved Acoustic Spectroscopy SLM (Hirsch et al., 2017) SRAS and Optical Microscopy Microstructure DED (Farshidianfar et al., 2017) DED (Farshidianfar et al., 2021a) DED (Gerchik et al., 2023) Thermography Thermography Thermal camera DED (Su et al., 2023b) Thermography Thermography Thermal camera DED (Su et al., 2020b) Thermography Thermography Thermal camera DED (Farshidianfar et al., 2020b) Thermography Thermal camera Phase transformation, grain size, melt pool width O.15 mm/pixel, 100 FPS DED (Farshidianfar et al., 2019) Spatially Resolved Acoustic Spectroscopy Pulsed Generation Laser, Mask, Detection Laser, Mask, De				Laser Doppler Vibrometer	Lack of fusion pores	12.5 MHz, spatial resolution 0.5 mm
SLM (Hirsch et al., 2018) Spatially Resolved Acoustic Spectroscopy SLM (Hirsch et al., 2017) SRAS and Optical Microscopy Pulsed Generation Laser, Mask, Detection Laser, Mask, Detection Laser, Mask, Detection Laser, Mask, Detection Surface Defects (Cracks, Pores) 10 μm Microstructure DED (Farshidianfar et al., 2017) DED (Farshidianfar et al., 2021a) Thermography IR sensor Cooling rate, grain structure, microhardness 0.5 mm/pixel, 30 Hz DED (Chechik et al., 2023) Thermography Thermal camera Grain area, average hardness 5.4 μm/pixel, 75 FPS DED (Su et al., 2022b) Thermography Thermal camera Phase transformation, grain size, melt pool width 0.15 mm/pixel, 1000 FPS SLM (Pieris et al., 2019) Spatially Resolved Acoustic Spectroscopy SLM (Smith et al., 2014) Spatially Resolved Acoustic Spectroscopy Pulsed Generation Laser, Mask, Detection Laser, Mask, Detection Laser, and Knife Edge Detector Microstructure Imaging and Grain Orientation 20 μm		SLM (Davis et al., 2019)	Laser Ultrasonic Imaging	Two-wave mixing interferometer	Lack of fusion pores	63 μm
Spectroscopy Laser, and Knife Edge Detector SLM (Hirsch et al., 2017) SRAS and Optical Microscopy Pulsed Generation Laser, Mask, Detection Laser, and Knife Edge Detector DED (Farshidianfar et al., 2021a) DED (Farshidianfar et al., 2021b) DED (Farshidianfar et al., 2023) Thermography IR sensor Cooling rate, grain structure, microhardness 0.5 mm/pixel, 30 Hz DED (Chechik et al., 2023) Thermography Thermal camera Grain area, average hardness 5.4 μm/pixel, 75 FPS DED (Su et al., 2022b) Thermography Thermal camera Phase transformation, grain size, melt pool width 0.15 mm/pixel, 1000 FPS DED (Farshidianfar et al., 2016) SLM (Pieris et al., 2019) Spatially Resolved Acoustic Spectroscopy SLM (Smith et al., 2014) Spatially Resolved Acoustic Spectroscopy Pulsed Generation Laser, Mask, Detection Laser, Mask, Detection Laser, and Knife Edge Detector Microstructure Imaging and Grain Orientation 20 μm		SLM (Honarvar et al., 2021)		Ultrasonic Transducer	Internal defects	0.132 mm at 50 MHz
Microstructure DED (Farshidianfar et al., 2021a) DED (Farshidianfar et al., 2021b) DED (Farshidianfar et al., 2023) DED (Su et al., 2022b) DED (Su et al., 2022b) DED (Farshidianfar et al., 2016) DED (Farshidianfar et al., 2019) Spatially Resolved Acoustic Spectroscopy SLM (Smith et al., 2014) Spatially Resolved Acoustic Spectroscopy Laser, and Knife Edge Detector Cooling rate, grain structure, microhardness 0.5 mm/pixel, 30 Hz Cooling rate, grain structure, microhardness 0.5 mm/pixel, 30 Hz Cooling rate, grain structure, microhardness 0.5 mm/pixel, 30 Hz Cooling rate, grain structure, microhardness 0.5 mm/pixel, 30 Hz Phase transformation, grain size, melt pool width 0.15 mm/pixel, 1000 FPS Microstructure variations Morphology-Surface and subsurface pores SLM (Smith et al., 2014) Spatially Resolved Acoustic Spectroscopy Pulsed Generation Laser, Mask, Detection Laser, Mask, Detecti		SLM (Hirsch et al., 2018)			Surface defects	10 μm/pixel
DED (Farshidianfar et al., 2021b) DED (Chechik et al., 2023) Thermography Thermal camera DED (Su et al., 2022b) Thermography Thermal camera Thermal camera DED (Farshidianfar et al., 2023) Thermography Thermal camera Phase transformation, grain size, melt pool width 0.15 mm/pixel, 1000 FPS DED (Farshidianfar et al., 2016) Thermography IR sensor Melt pool temperature, dilution, clad height 0.5 mm/pixel SLM (Pieris et al., 2019) Spatially Resolved Acoustic Spectroscopy Spatially Resolved Acoustic Spectroscopy SLM (Smith et al., 2014) Spatially Resolved Acoustic Spectroscopy Pulsed Generation Laser, Mask, Detection		SLM (Hirsch et al., 2017)			Surface Defects (Cracks, Pores)	10 μm
DED (Chechik et al., 2023) Thermography Thermal camera Grain area, average hardness 5.4 μm/pixel, 75 FPS DED (Su et al., 2022b) Thermography Thermal camera Phase transformation, grain size, melt pool width 0.15 mm/pixel, 1000 FPS DED (Farshidianfar et al., 2016) SLM (Pieris et al., 2019) Spatially Resolved Acoustic Spectroscopy Spatially Resolved Acoustic Spectroscopy Spatially Resolved Acoustic Spectroscopy Pulsed Generation Laser, Mask, Detection Laser, Mask, Detection Laser, Mask, Detection Detector Laser, and Knife Edge Detector Microstructure variations Morphology-Surface and subsurface pores Microstructure lmaging and Grain Orientation 20 μm	Microstructure		Thermography	IR sensor	Cooling rate, grain structure, microhardness	0.5 mm/pixel, 30 Hz
DED (Su et al., 2022b) Thermography Thermal camera Phase transformation, grain size, melt pool width 0.15 mm/pixel, 1000 FPS DED (Farshidianfar et al., 2016) Thermography IR sensor Melt pool temperature, dilution, clad height 0.5 mm/pixel SLM (Pieris et al., 2019) Spatially Resolved Acoustic Spectroscopy SLM (Smith et al., 2014) Spatially Resolved Acoustic Spectroscopy Pulsed Generation Laser, Mask, Detection Laser, and Knife Edge Detector Microstructure variations Morphology-Surface and subsurface pores SLM (Smith et al., 2014) Spatially Resolved Acoustic Spectroscopy Pulsed Generation Laser, Mask, Detection Laser, and Knife Edge Detector Microstructure Imaging and Grain Orientation 20 µm			Thermography	IR sensor	Cooling rate, grain structure, microhardness	0.5 mm/pixel, 30 Hz
DED (Farshidianfar et al., 2016) SLM (Pieris et al., 2019) Spatially Resolved Acoustic Spectroscopy SLM (Smith et al., 2014) Spatially Resolved Acoustic Spectroscopy Pulsed Generation Laser, Mask, Detection Laser, Mask, Detection Laser, Mask, Detection Detector Pulsed Generation Laser, Mask, Detection Detector SLM (Smith et al., 2014) Spatially Resolved Acoustic Spectroscopy Pulsed Generation Laser, Mask, Detection Detector Pulsed Generation Laser, Mask, Detection Detector Microstructure Imaging and Grain Orientation 20 μm		DED (Chechik et al., 2023)	Thermography	Thermal camera	Grain area, average hardness	5.4 μm/pixel, 75 FPS
SLM (Pieris et al., 2019) Spatially Resolved Acoustic Spectroscopy Pulsed Generation Laser, Mask, Detection Laser, Mask, Detection pores SLM (Smith et al., 2014) Spatially Resolved Acoustic Spectroscopy Pulsed Generation Laser, Mask, Detection Microstructure variations Morphology-Surface and subsurface pores Pulsed Generation Laser, Mask, Detection Microstructure Imaging and Grain Orientation 20 μm Laser, and Knife Edge Detector		DED (Su et al., 2022b)	Thermography	Thermal camera	Phase transformation, grain size, melt pool width	0.15 mm/pixel, 1000 FPS
Spectroscopy Laser, and Knife Edge Detector SLM (Smith et al., 2014) Spatially Resolved Acoustic Spectroscopy Pulsed Generation Laser, Mask, Detection Laser, Mask Detection Laser, and Knife Edge Detector Pulsed Generation Laser, Mask Detection Microstructure Imaging and Grain Orientation 20 μm		DED (Farshidianfar et al., 2016)	Thermography	IR sensor	Melt pool temperature, dilution, clad height	0.5 mm/pixel
Spectroscopy Laser, and Knife Edge Detector		SLM (Pieris et al., 2019)				-
		SLM (Smith et al., 2014)			Microstructure Imaging and Grain Orientation	20 μm
SLM (Patel et al., 2018) Spatially Resolved Acoustic Pulsed Generation Laser, Mask, Detection Microstructure (Image 1 exture) and Morphology - Surface U.35 µm/pixel Spectroscopy Laser, and Knife Edge Detector Roughness		SLM (Patel et al., 2018)	Spatially Resolved Acoustic Spectroscopy	Pulsed Generation Laser, Mask, Detection Laser, and Knife Edge Detector	Microstructure (Image Texture) and Morphology - Surface Roughness	0.35 μm/pixel
SLM (Sharples et al., 2006) Spatially Resolved Acoustic Spectroscopy Pulsed Generation Laser, Mask, Detection Laser, and Knife Edge Detector Microstructure of multi-grained materials 0.8 mm		SLM (Sharples et al., 2006)			Microstructure of multi-grained materials	0.8 mm
SLM (Lu et al., 2022) Optical Powder bed scanner Build density 20 µm/pixel		SLM (Lu et al., 2022)	Optical	Powder bed scanner	Build density	20 μm/pixel
EBM (Gardifiell et al., 2023) Electron optical imaging Backscattered Electron Powder contamination 1,500 × 1,500 pixel*, 20 MHz		EBM (Gardfjell et al., 2023)	Electron optical imaging	Backscattered Electron	Powder contamination	1,500 × 1,500 pixel*, 20 MHz

(Continued on following page)

TABLE 1 (Continued) Imaging techniques used in different fusion-based additive manufacturing processes.

Aspects	AM process	lmaging technique	Sensor	Feature	Spatial and temporal resolution
	EBM (Wong et al., 2019)	Electron optical imaging	Backscattered Electron	Quality	1800 × 1800 pixels*, 118.8 KHz
	DED (Freeman et al., 2023)	Optical	CMOS	Flexural stress-strain curves	5.4 μm/pixel, 28 FPS
	EB-DED (Liang et al., 2022; Liang et al., 2023)	Optical	Industrial camera	Absorbed current	640 × 480 pixels*, 50 FPS

^aCamera resolution.

The generation of high-quality image data for training machine learning and AI models is expensive, posing a challenge for industries to widely adopt such techniques. Even with advancements in imaging technology leading to cheaper options that maintain high image quality, processes such as storage and labeling of such high-resolution datasets are highly resource-intensive, further straining a company's finances. However, ML/AI methods have evolved to enable the extraction of valuable insights even from low-quality image data. Techniques such as transfer learning and data augmentation have provided the means for artificial data generation and training more robust models with less pristine data.

While there are still some restrictions on the widespread adoption of in-situ imaging techniques, they offer a plethora of advantages over other sensing modalities. They provide highresolution visual data that works exceptionally well with modern deep learning architectures while also being human-friendly for quick human decision-making or intervention. Intricate visual patterns and anomaly detection are possible, which might evade detection via other sensing technologies. In-situ imaging also provides more flexibility and adaptability when it comes to reproducing the same setup elsewhere, making them versatile for various applications. Most other sensing modalities require some amount of contact with the process or the machine, while these machine vision-based in-situ methods provide for non-contact measurements and monitoring. Such methods also relax the need for specialized signal conditioning or data acquisition system requirements by often providing plug-and-play usage.

The subsequent sections of this paper are structured as follows: Section 2 comprises a comprehensive literature review as listed in Table 1 that specifically concentrates on imaging techniques employed within the field of additive manufacturing. Moreover, detailed case studies are provided in Section 3, showcasing experiments carried out on DED process at Texas A&M University. *In-situ* imaging methods are discussed, about the utilization of high-speed cameras, thermal cameras, and digital cameras for real-time observation and analysis. Furthermore, comprehensive exploration is undertaken on post-processing imaging techniques, specifically highlighting the application of 3D optical profilometry and the image segmentation toolbox for defect detection. Concluding remarks are presented in Section 4.

2 Overview of imaging methods for fusion-based additive manufacturing

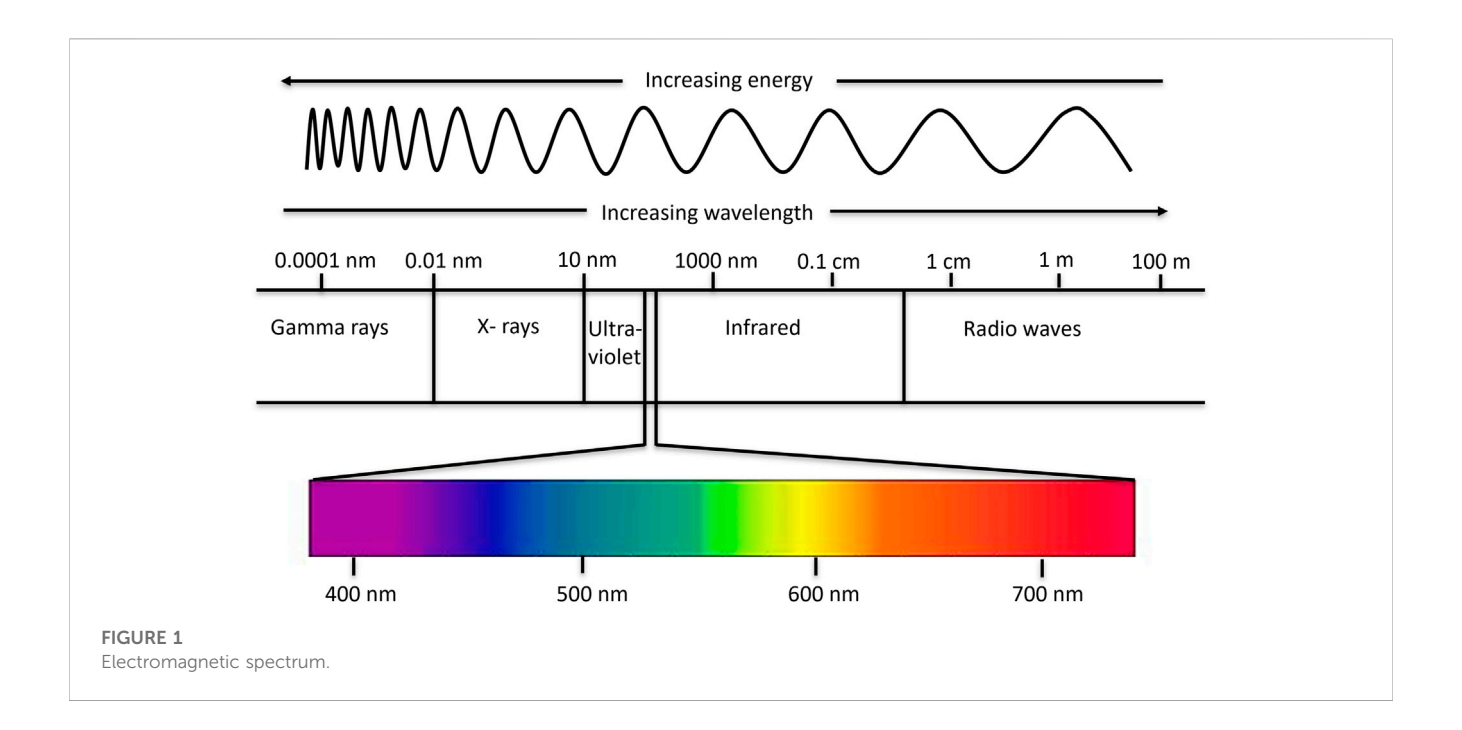
This section evaluates key optical sensing technologies in literature for *in-situ* imaging measurements in additive

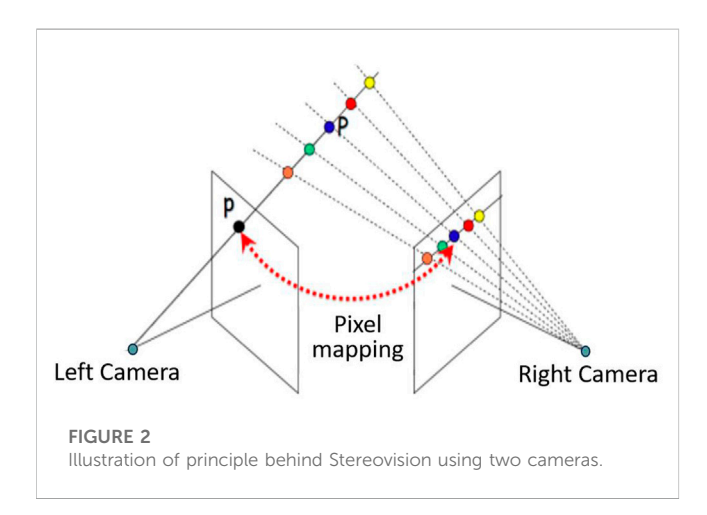
manufacturing. The imaging techniques are classified based on the type of wave used for imaging: electromagnetic waves (see Figure 1) and mechanical waves (e.g., laser ultrasonic and spatially resolved acoustic spectroscopy imaging). While not exhaustive, the primary focus is on the most significant imaging techniques that offer high-resolution capture of process physics and integration with machine learning and artificial intelligence methods during model training. The objective is to assess the capabilities and performance of these technologies in a scientific context and to highlight their utility for non-destructive evaluation of surface characteristics during additive manufacturing.

Radio waves, characterized by longer wavelengths and lower frequencies relative to other forms of electromagnetic radiation, are not a preferred choice for high-resolution imaging in additive manufacturing. Although their propensity to traverse large distances renders them suitable for communication and data transmission, their interaction with matter does not facilitate non-destructive evaluation and process monitoring in additive manufacturing. Conversely, gamma rays, characterized by extremely short wavelengths and high frequencies are highly energetic. While gamma rays have the ability to penetrate deep into materials and can be used for non-destructive testing, their adoption in additive manufacturing for *in-situ* process monitoring is limited due to safety concerns.

2.1 X-ray imaging

High speed X-ray imaging and X-ray diffraction studies for insitu characterization of Laser Bed Powder Fusion (LBPF) process have revealed several significant phenomena such as melt pool dynamics, solidification rates, phase transformation and pore formation mechanism due to keyhole at high spatial and temporal resolutions (Zhao et al., 2017; Leung et al., 2018). Wolff et al. illustrated the use of high-speed synchrotron hard X-ray imaging to study the pore formation dynamics in DED with micrometer spatial resolution and microsecond temporal resolution as shown in Figure 2. Due to the inherent difference in the way DED and LBPF systems are designed, the pore formation dynamics differ for both the processes. Particle deposition was found to be the key driver behind pore formation due to lack of fusion in DED and the presence of voids between the packed particles on the powder bed was the primary reason for porosity due to lack of fusion in LPBF (Wolff et al., 2021a; Wolff et al., 2021b). Owing to the difficulties for X-ray passage in commercial PBF systems, Bidare et al. designed an open architecture for metal PBF system accommodating for two X-ray imaging directions and the entire set up being easily transportable allowing for

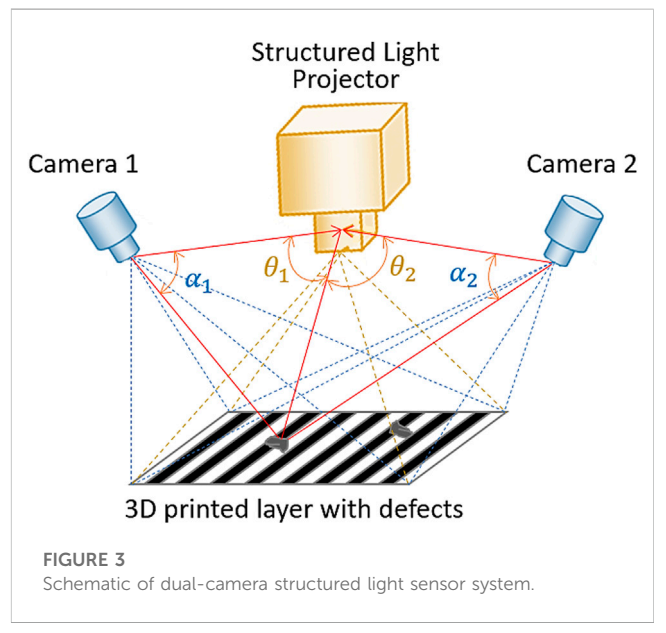




inspections at different measurement facilities (Bidare et al., 2017). The widespread adoption of *in-situ* X-ray imaging for DED and other AM processes at an industrial scale faces several challenges. High costs are a significant deterrent, and the requirement for a complex setup that demands regular adjustments complicates operational procedures. Furthermore, environmental factors, such as ionizing radiation, as well as material-specific properties such as emissivity and reflectivity, pose additional challenges to its applicability.

2.2 Optical imaging (visible spectra)

Optical methods that utilize electromagnetic waves in the visible spectrum are among the most frequently employed *in-situ* monitoring systems for additive manufacturing. These methods leverage different types of detectors to capture high-speed images



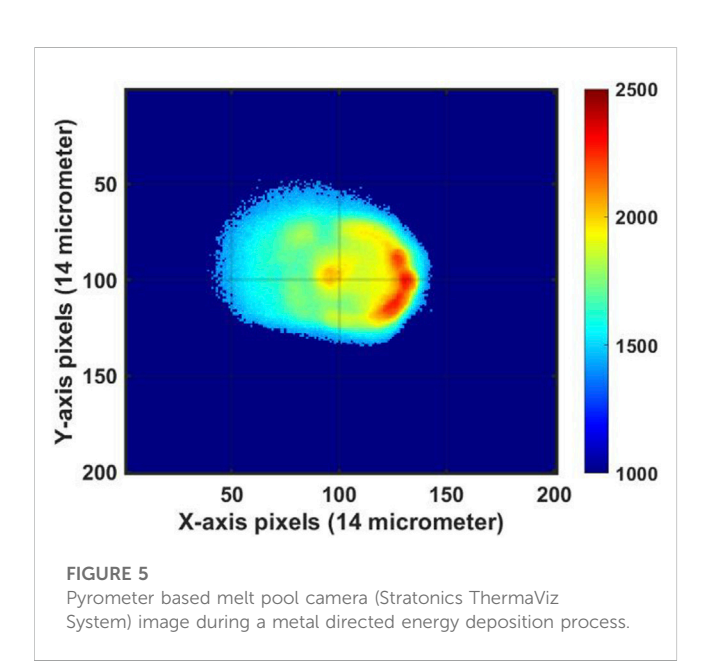
of the process, providing valuable insights into the material deposition and quality assurance aspects of additive manufacturing.

2.2.1 Stereovision

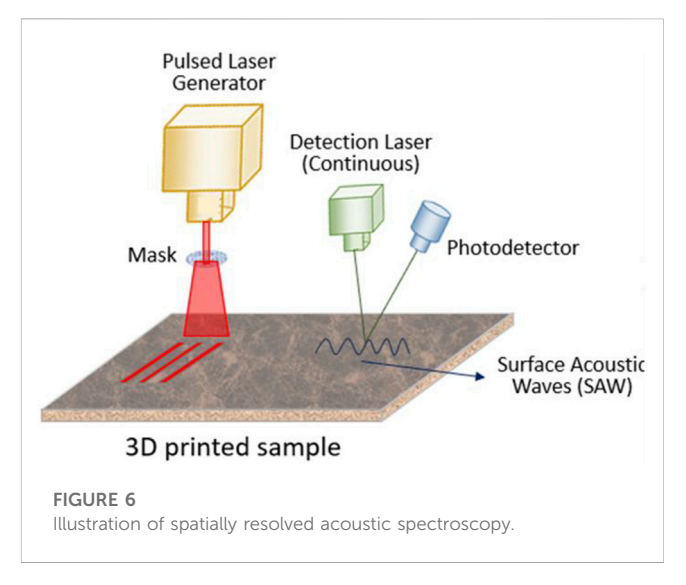
Stereo vision is a method for reconstructing the 3-D structure of an object from corresponding points from 2 cameras by triangulation. Based on the configuration of the cameras and their intrinsic parameters, one can calibrate the "line of sight" of each pixel, and the intersection of the corresponding lines of sight from both the cameras will help us infer the 3-D position as shown in Figure 3 (Lazaros et al., 2008; Kanatani et al., 2008). With respect



FIGURE 4
High speed camera image during a metal directed energy deposition process.



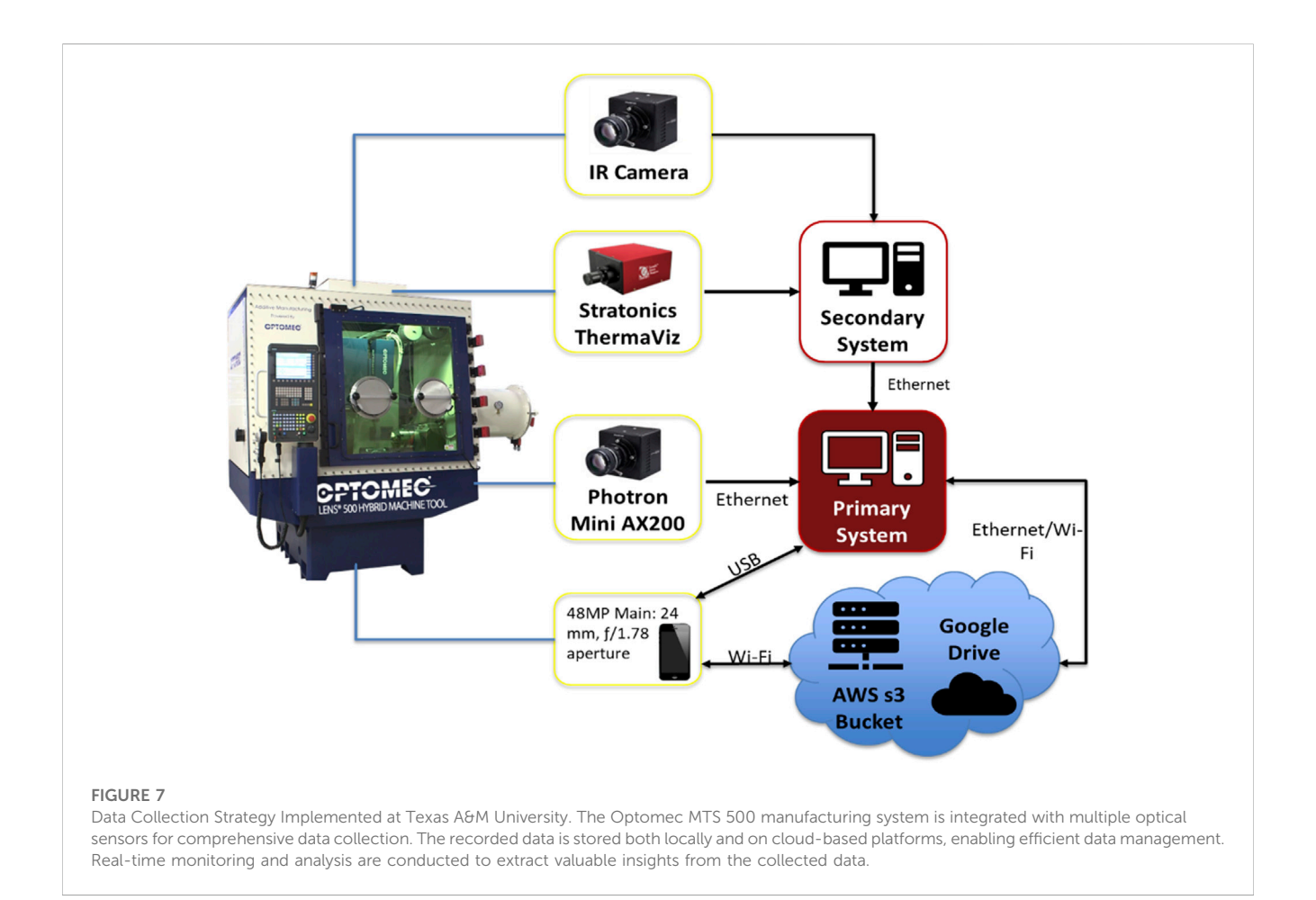
to metal AM, stereovision can help capture the geometry of melt pool and identify the size, speed, direction, and age of spatter ejected from the laser melt pool (Eschner et al., 2020). Barrett *et al.*, employed a stereovision camera system to record the selective laser melting of maraging steel, with two cameras in 1,000 fps setting having $1,280 \times 720$ -pixel count resulting in a spatial resolution of about $20 \, \mu \text{m/pixel}$. The cameras were synchronized to measure stereoscopic features of the resulting spatter. Laser spatter can help us infer the process and quality of the part being built *in-situ* with a qualify-as-you-go methodology (Barrett et al., 2019; Barrett et al., 2018a). Liu *et al.* investigated a stereo vision-based system for a hybrid (additive and subtractive) manufacturing



process to automatically detect the defect area and generate a tool path for repairing the defect (Liu et al., 2017). The resolution of the cameras and proper illumination will act as a bottleneck as we aim to characterize surfaces corresponding to different materials in the submicron scale.

2.2.2 Structured light systems (SLS)

The principle of structured-light 3D surface imaging technique is to extract the 3D surface shape based on the information from the distortion of the projected structured-light pattern. The distortions of the fringe pattern due to variations in surface height of the sample can be precisely captured by the cameras. SLS utilizes the triangulation principle to calculate the relative positions of the measuring points on the target surface. The use of multiple fringe patterns and the corresponding reconstruction improves the measurement accuracy of this technique without compromising speed compared to other methods, and therefore is suited for in-situ AM applications as shown in Figure 3 (Zhang et al., 2020; Wang et al., 2021). A dual-camera SLS consists of two cameras and a projector. Usually, the projector acts as a bottleneck in the set up with respect to the resolution. However, implementation of phase shifting method and defocusing technique on the multiple fringe patterns can compensate the shortcomings of the projector resolution, as demonstrated by Wang et al. They were able to achieve a spatial resolution measurement of 5 µm with an accuracy of 0.05 µm, by using 6 different fringe patterns (Wang et al., 2021). Zhang et al. employed a custom designed single projector single camera fringe projection system for in situ metrology in Laser Powder Bed Fusion (LBPF) process. They were able to achieve a spatial resolution of 6.8 µm/pixel and a single point repeatability measure of 0.47 μm for measuring the surface topography at each layer using phase shifting and unwrapping algorithms (Zhang et al., 2016). Li et al. proposed a 4D line-scan hyperspectral imager by employing a camera with a spectrograph for a line-scan fringe projection (c) profilometry and achieved a spectral resolution of 2.8 nm along with the spatial root mean square error of 0.0895 nm when measuring a sphere of diameter 40.234 nm (Li et al., 2021a). Harshavardhan et al. proposed a new fringe projection method



using polarized light illumination and a polarization camera which could measure moving objects or varying shape objects with high speed (Harshavardhan et al., 2018).

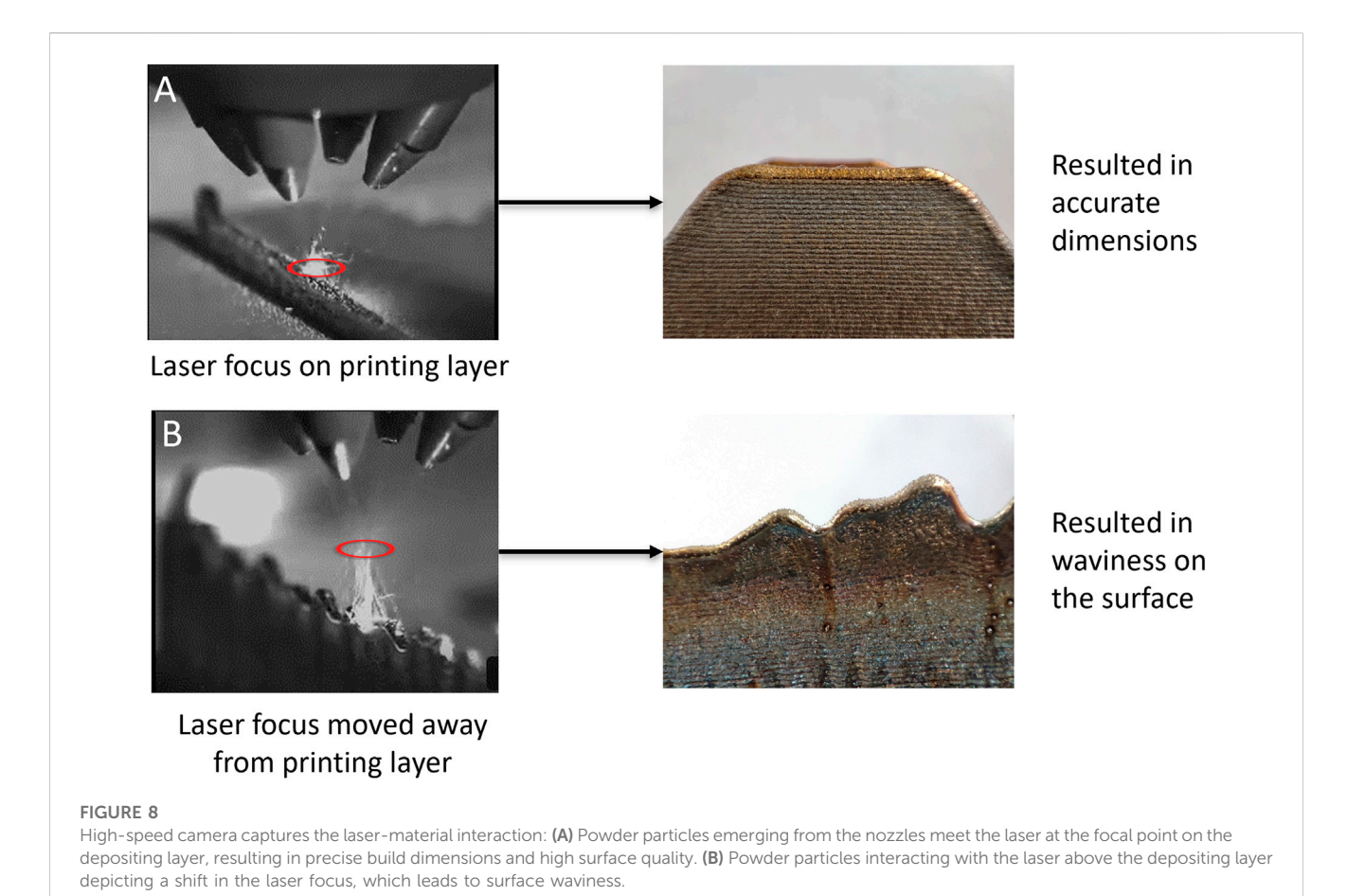
2.2.3 Optical coherence interferometry

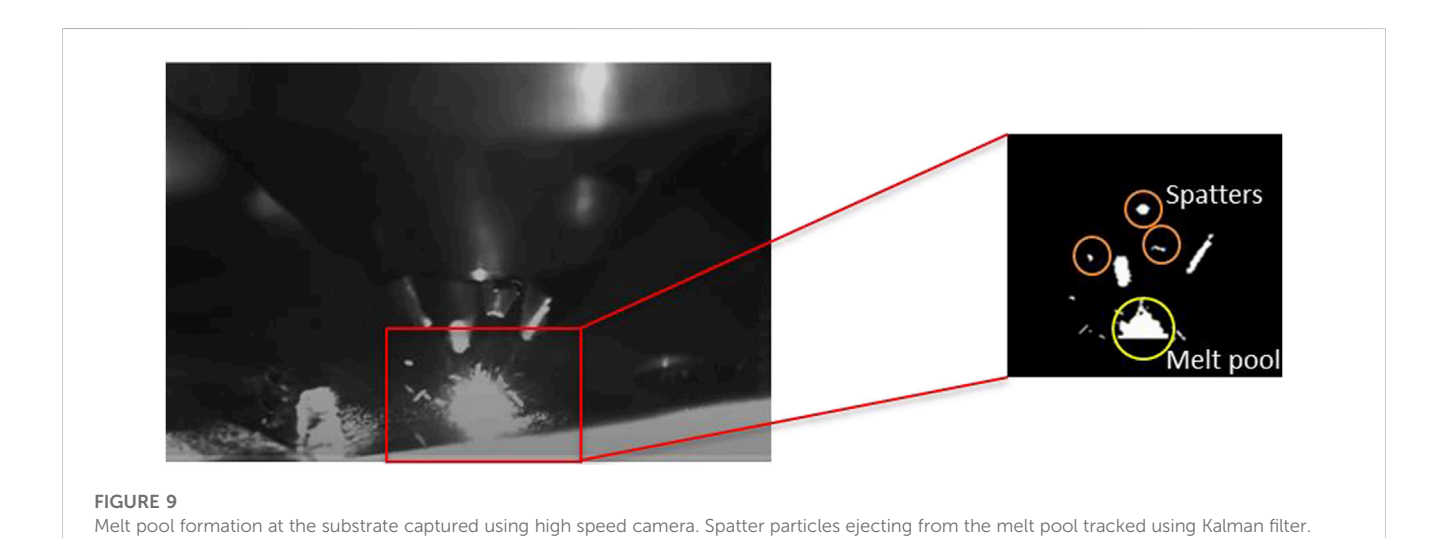
Interferometry captures the depth information of the surface under study by using the interference pattern of two coincident light beams that travel unequal paths. An important characteristic of the interferometric surface topography measurement is that the sensitivity to variations in the measurement is independent of the field of view unlike other optical metrology techniques involving triangulation, fringes or focus effects (De Groot, 2019). However, the surface under consideration needs to be reflective in nature to obtain accurate measurements. The resolution of interferometers is generally in the order of 10 nm in the longitudinal direction and in the order of 1 µm in the lateral direction (Gomez et al., 2020). Optical Coherence Tomography (OCT) is essentially a low coherence interferometer, samples points in the depth direction and constructs a cross sectional image (Yoshizawa, 2009). Spectraldomain optical coherence tomography (SD-OCT) techniques have been reported in literature for monitoring real time in-situ melt pool morphology changes and surface roughness measurements for each layer in LPBF processes (DePond et al., 2018; Kanko et al., 2016). The interference spectrogram, recorded by a 100 kHz Si CMOS camera is then transformed into a map of intensity as a function of distance above the powder bed surface. SD-OCT has been found to

permit a long working distance, high sampling rate and provides micrometer scale axial and lateral resolution.

2.2.4 Optical displacement sensors

High accuracy optical displacement sensors can be categorized into two types depending on their working principle being laser triangulation and confocal imaging. Laser profilers (or) laser displacement sensors are used to collect height data across a laser line on the surface instead of a single point. A common example would be the Kinect sensor, which uses an Infra-Red (IR) projector to project a pattern of IR dots onto the surface under consideration and the reflected rays are captured by a monochrome CMOS camera placed a few centimeters apart. The depth information is estimated using the principles of triangulation. In the field of additive manufacturing, Barrett et el. employed a high-resolution laser line profilometer to provide a micron level surface map of each layer after being printed in a LPBF system (Barrett et al., 2018b). Wang et al. employed a stereovision camera coupled with a laser displacement sensor for a hybrid manufacturing setup with CNC milling to achieve a spatial resolution of the order of 10 µm (Wang et al., 2015). Confocal sensors use a white light source that is focused onto the target surface by a multi-lens optical system. The objective of the multi-lens system is to disperse the light into monochromatic stages along the measurement axis. A specific distance to the target is assigned to each color's





wavelength in a factory calibration. The distance or surface topography is accurately captured by detecting the colors from the reflected light (Fu et al., 2020). Confocal sensors are used when laser displacement sensors do not make a measurement either due to the type of material used such as one-sided glass or if measurements need to be captured in tiny spaces in the sub-micron scale.

2.2.5 Digital camera

Optical metrology techniques can help real time *in-situ* monitoring of the workpiece surface morphology evolution and tool condition because of their non-contact nature. Digital cameras involving CCD (charge-coupled device), or CMOS (complementary metal oxide semiconductor) technology have been reported in literature for *in-situ* monitoring of surfaces during machining

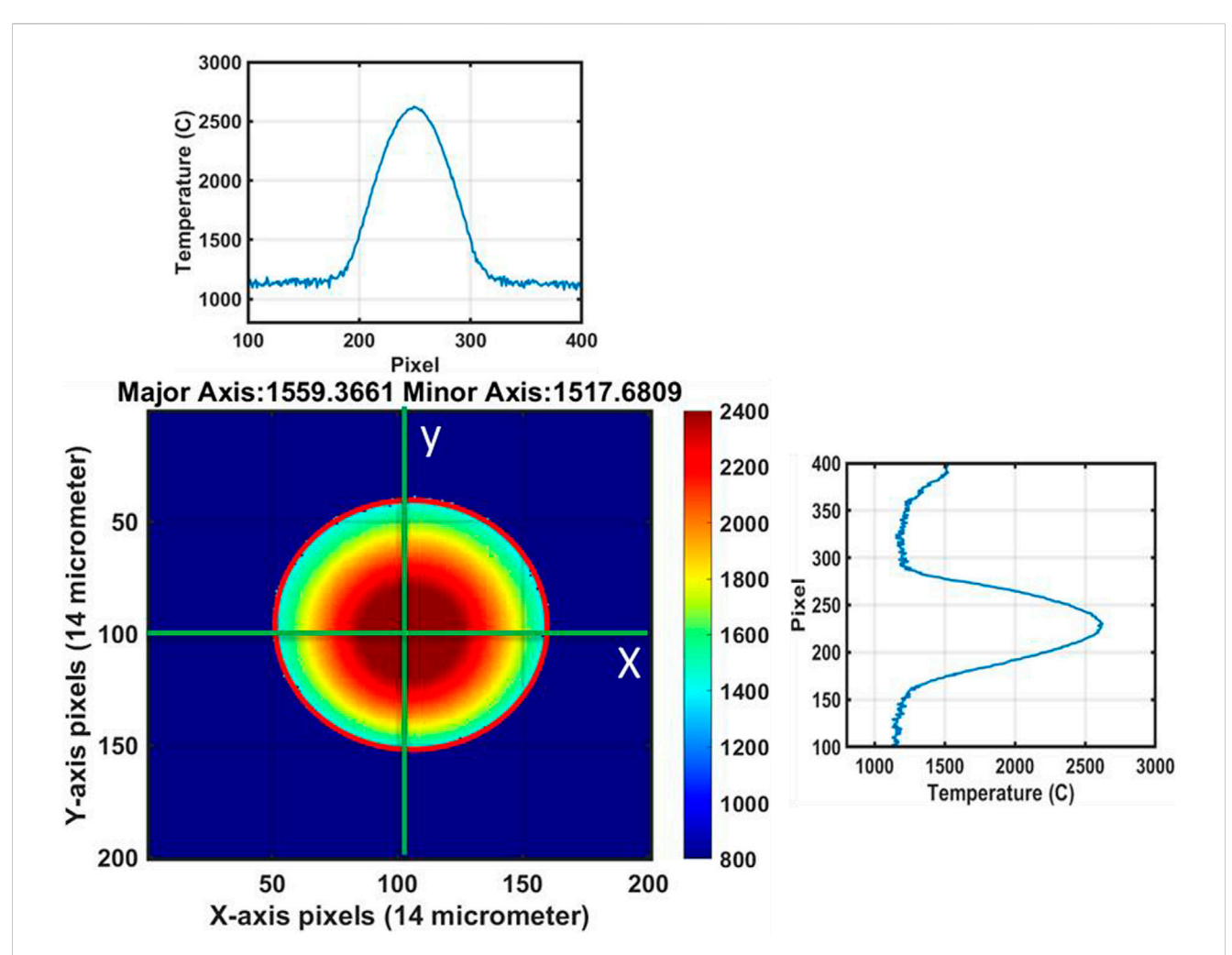


FIGURE 10
Melt pool geometry, with major axis and minor dimensions calculated using melt pool frames captured by the thermal camera. Additionally, the temperature distribution curve along the x-y direction exhibits a smooth profile, indicating uniform heat distribution within the melt pool and ensuring the absence of anomalies during the deposition process.

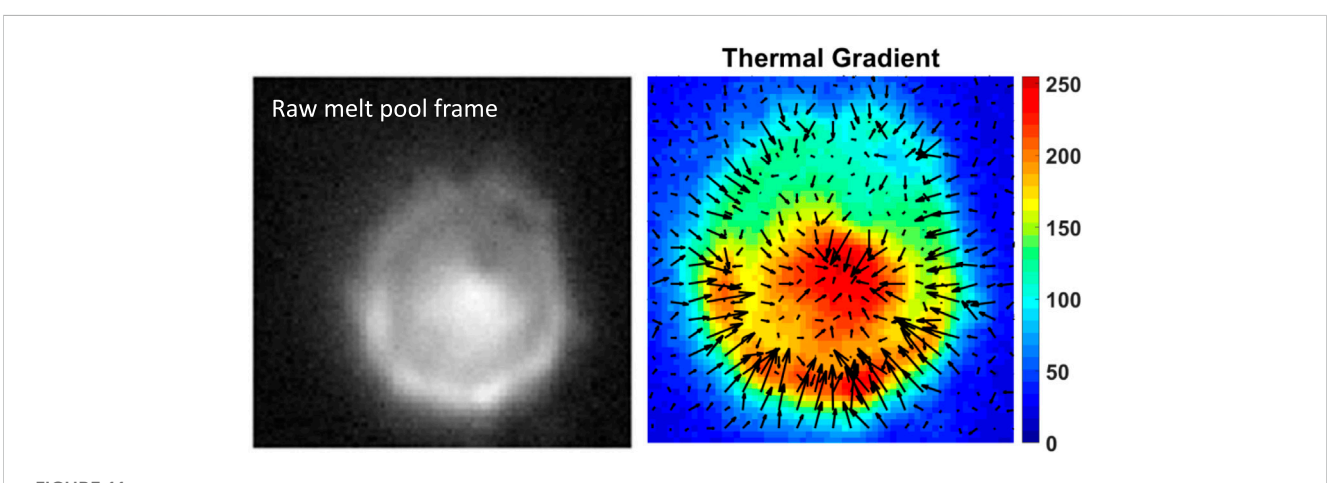


FIGURE 11
A custom MATLAB algorithm used to calculate the thermal gradients from the raw melt pool frame. Quiver plots depict the temperature decrease from the edge of the melt pool towards its center, representing a crucial step in the formation of ripples DED process.



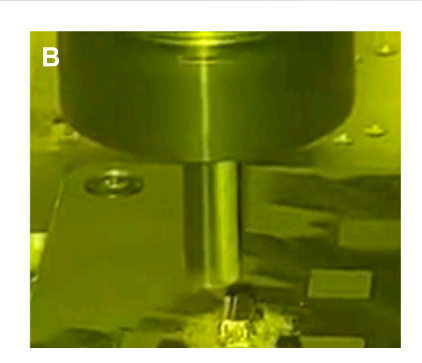


FIGURE 12
A smartphone digital camera recording (A) laser material deposition during the printing cycle, (B) milling operation carried out after printing in Hybrid DED process.

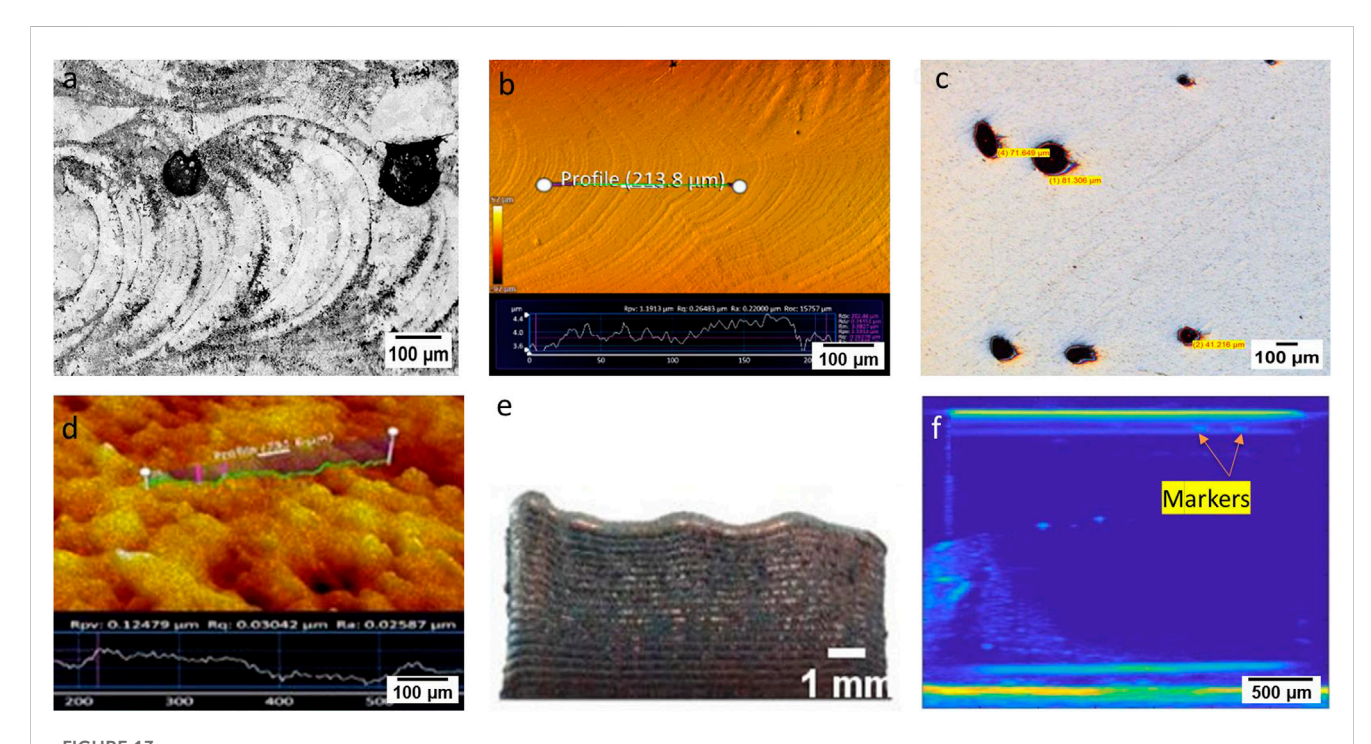


FIGURE 13
(A) SEM micrographs showing the formation of cellular structure in the DED printed 316L components, (B) 3D optical profilometer capturing the surface morphology (ripples) and their Ra variation along the scan track, (C) optical micrograph showing voids and pores spread across the scan surface of DED-printed component (D,E) surface waviness captured using 3D optical profilometer, (F) artifacts captured using ultrasound imaging.

operations. All the pixel's signals are processed by a single circuit or chip in a CCD camera, whereas a CMOS camera has a processing circuit for each pixel which improves speed but reduces the capture area due to increased complexity (Tapia and Elwany, 2014). Challenges associated with the use of CCD or CMOS include the requirement for high frame rate of capture for continuous streaming and post processing of images in order to extract useful information.

With the rapid development of machine vision, image processing and pattern recognition methods, advanced optical solutions are combined with machine learning technologies for surface defect detection and characterization. Iravani *et al.* set up an optical system for AM comprising of 3 CCD cameras at 120° apart relative orientation over the substrate plane and used a recurrent

neural network model to monitor the layer heights using the images from the CCD cameras (Iravani-Tabrizipour and Toyserkani, 2007). Image segmentation methods and deep learning networks including CNN (Convolutional Neural Networks) and ensemble models have been developed on surface images obtained during additive manufacturing and post processing operations for defect detection and roughness estimation (Gobert et al., 2018; Liu et al., 2019; Giusti et al., 2020; Qi et al., 2020).

2.2.6 High speed digital cameras

High speed digital cameras (see Figure 4) have been found suitable for real time *in-situ* monitoring of melt pool formation, spatter particle tracking and surface porosity in additive

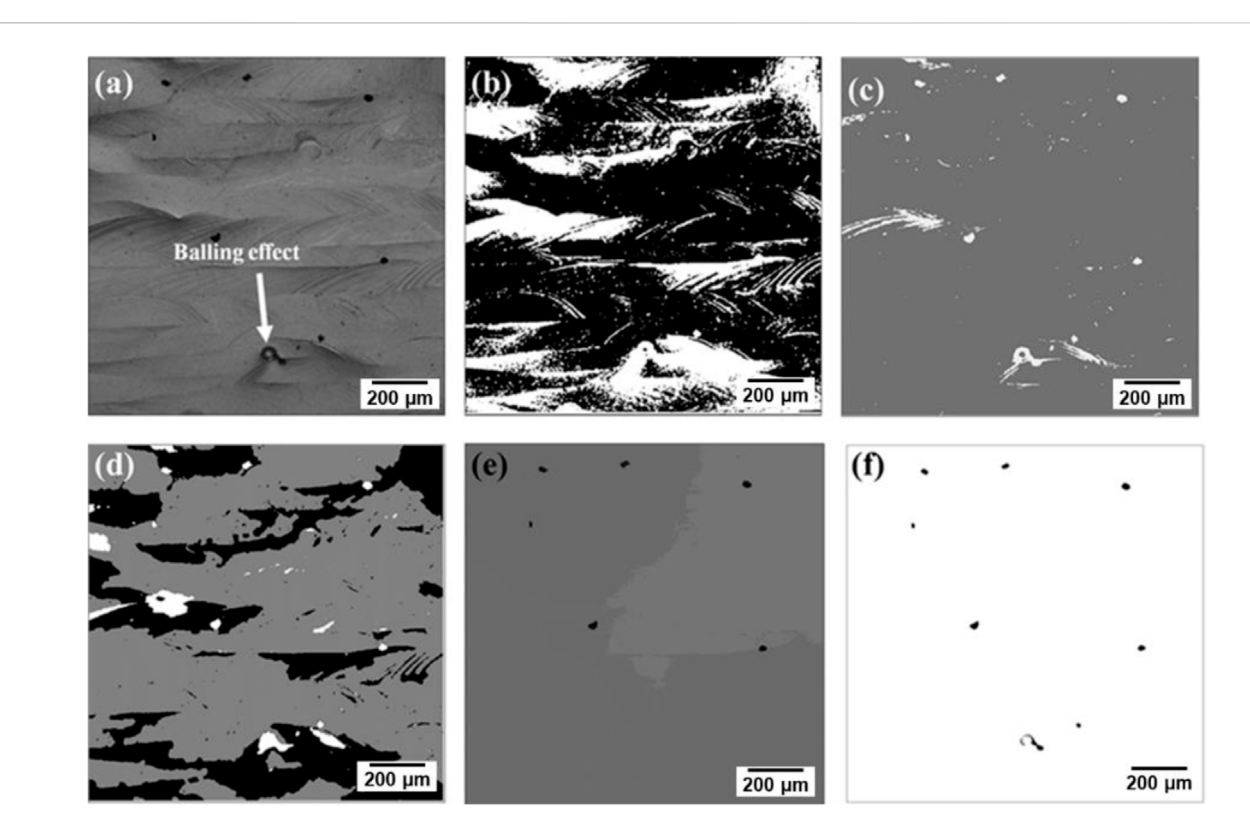


FIGURE 14
Comparative results of different algorithms tested for the segmentation of defects. (A) Original image for sample A (B) k-means with 2 clusters (C)
Gaussian mixture model with expectation maximization (D) spatially constrained Gaussian mixture model with k-means initialization and (E) mean shift (F) proposed method (Iguebal and Bukkapatnam, 2022).

manufacturing. The setup of a high-speed camera involves selecting the right camera based on factors like frame rate and resolution. Proper lighting sources are positioned for adequate illumination, especially in high-speed scenarios. A stable mounting system minimizes vibrations, and synchronization with external devices ensures precise timing for capturing fast events. Frame rates in the range of 1,000 fps to 6,000 fps have been reported on multiple occasions in literature to characterize melt pool dynamics and particle behavior (You et al., 2014; Andani et al., 2017; Repossini et al., 2017). Ly et al. used an ultra-high-speed camera with frame rate of 100,000 fps to discover the spatter causing phenomenon of vapor driven entrainment of microparticles by an ambient gas flow (Ly et al., 2017). Matilainen et al. used a high-speed camera with an active illumination system to monitor the laser interaction time and the formation of keyholes during additive manufacturing of stainless steel (Matilainen et al., 2015).

2.3 Infrared imaging

Next, we will delve into the topic of infrared-based monitoring systems. These systems utilize infrared radiation, a type of electromagnetic radiation with wavelengths longer than those of visible light, to capture information about the process or material under study. Infrared-based monitoring systems are commonly used in additive manufacturing for various applications, such as melt pool monitoring, temperature measurement, and defect detection.

2.3.1 Infrared (IR) camera

To set up an infrared (IR) camera the appropriate camera must be selected based on the desired temperature range and resolution. Calibration ensures accurate temperature measurement, and lens focus and alignment capture clear thermal images. Controlling ambient temperature and reducing reflective surfaces optimizes thermal contrast. Hu and Kovacevic (Hu and Kovacevic, 2003a) developed a closed-loop control system utilizing infrared (IR) imaging sensing to regulate heat input and the size of the melt pool in the Directed Energy Deposition (DED) process. By employing IR imaging, the resulting images were able to eliminate noise caused by metal powder and facilitate real-time processing. The captured IR images provided temperature information, a crucial parameter influencing the quality of the cladding outcome.

2.3.2 Pyrometer based melt pool camera

The setup of a pyrometer-based melt pool thermal camera (see Figure 5) involves calibrating the camera for accurate temperature measurements, and choosing the appropriate exposure based on the material's emissivity. The camera is positioned to capture clear thermal images, and optimal lighting conditions and thermal insulation are implemented. Data analysis software enables real-time monitoring and control of the melt pool temperature. Smoqi et al. (Smoqi et al., 2022) implemented a closed-loop control system in their study, utilizing the melt pool temperature as a feedback signal to adjust the laser power in the additive manufacturing

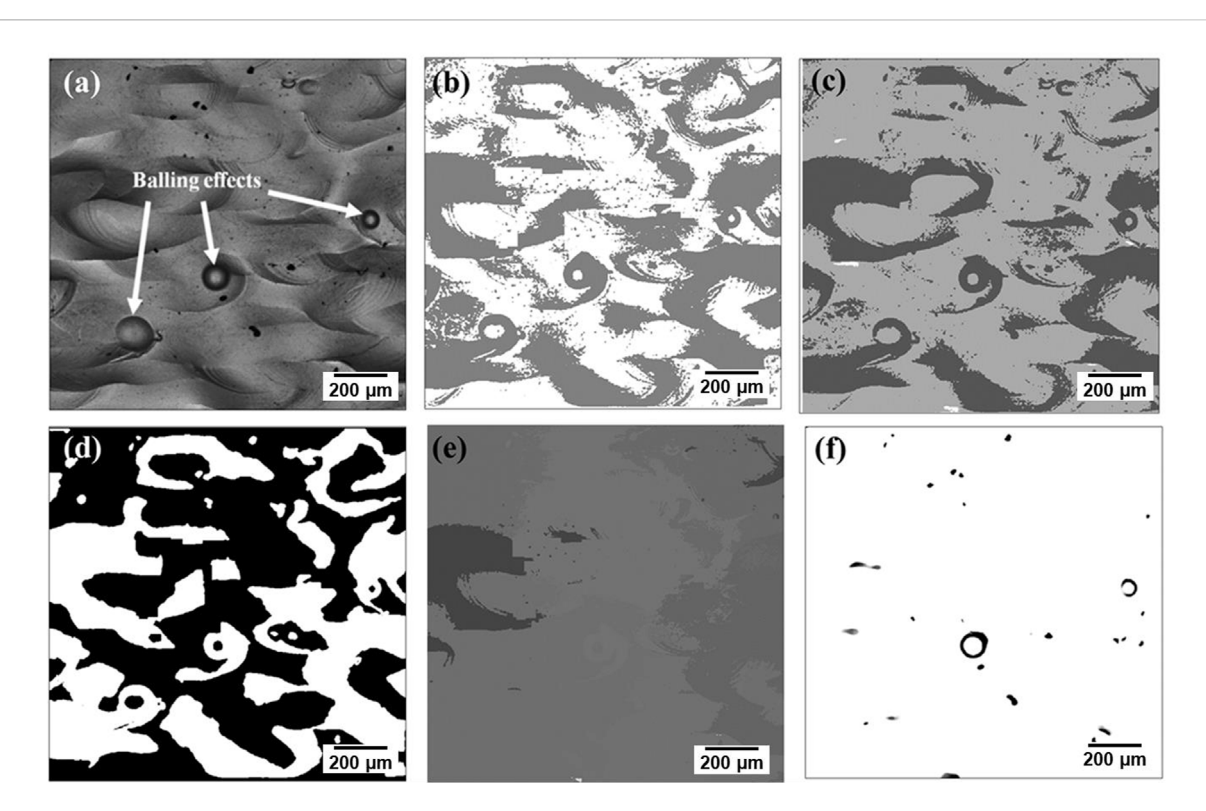


FIGURE 15
Comparative results of different algorithms tested for the segmentation of defects. (A) Original image for sample B (B) k-means with 2 clusters (C)
Gaussian mixture model with expectation maximization (D) spatially constrained Gaussian mixture model with k-means initialization and (E) mean shift (F) proposed method (Iquebal and Bukkapatnam, 2022).

process. They employed a two-wavelength pyrometer to provide the necessary feedback. The researchers reported that the volume porosity observed in components manufactured under the closed-loop control system ranged from 0.036% to 0.043%, which was lower than the range of 0.032%–0.068% observed in components manufactured under an open-loop control system.

2.4 Laser ultrasonic imaging

In addition to *in-situ* monitoring techniques that utilize electromagnetic waves, methods employing mechanical waves, such as laser ultrasonic imaging and spatially resolved acoustic spectroscopy, have emerged as highly effective non-destructive testing (NDT) methods. These methods are adept at detecting and evaluating surface, subsurface, and internal defects.

Laser Ultrasonic (LU) Imaging integrates the principles of laser generation and ultrasonic detection to yield high-resolution images of a material's interior. This technique has been predominantly used for characterizing the surface geometry and morphology of additively manufactured parts. The selection of Ultrasonic Testing (UT) methods for defect detection and material characterization in additive manufacturing largely depends on the manufacturing process, the material under examination, and the capabilities of UT techniques.

Spatially Resolved Acoustic Spectroscopy (SRAS) is a laser ultrasonic technique that employs Surface Acoustic Waves

(SAWs) to investigate the elastic properties of a component as shown in Figure 6 (Smith et al., 2014; Pieris et al., 2019). The SRAS system comprises a pulsed laser generator, a mask to define the acoustic wavelength, a continuous detection laser, and a Knife Edge Detector (KED). The generation laser, in conjunction with the mask, rapidly heats the sample within its thermoelastic regime, generating a SAW with a defined wavelength $\boldsymbol{\lambda},$ as determined by the fringe spacing imaged onto the sample surface. The frequency f of the SAW is measured by monitoring the perturbation of the detection laser via the KED. This translates to a measured wave velocity of $v = f\lambda$. The knife edge detector, also known as optical beam deflection, is a robust method for detecting ultrasonic waves using a laser. In the case of a specular reflection of the incident laser beam from a smooth surface, any lateral movement of the reflected beam caused by the ultrasonic waves is easily detected by a pair of photodiodes.

A major disadvantage of the knife edge detector is that it does not cope well with optically rough surfaces. The optical speckles from a rough surface adversely affect the efficiency of the knife edge detector, because 'dark' speckles move synchronously with 'bright' speckles, and their contributions to the ultrasonic signal cancel each other out. The SRAS method has demonstrated significant potential for comprehensive material characterization, enabling the assessment of not only surface defects but also grain orientation and microstructures (Sharples et al., 2006; Hirsch et al., 2017; Hirsch et al., 2018; Patel et al., 2018).

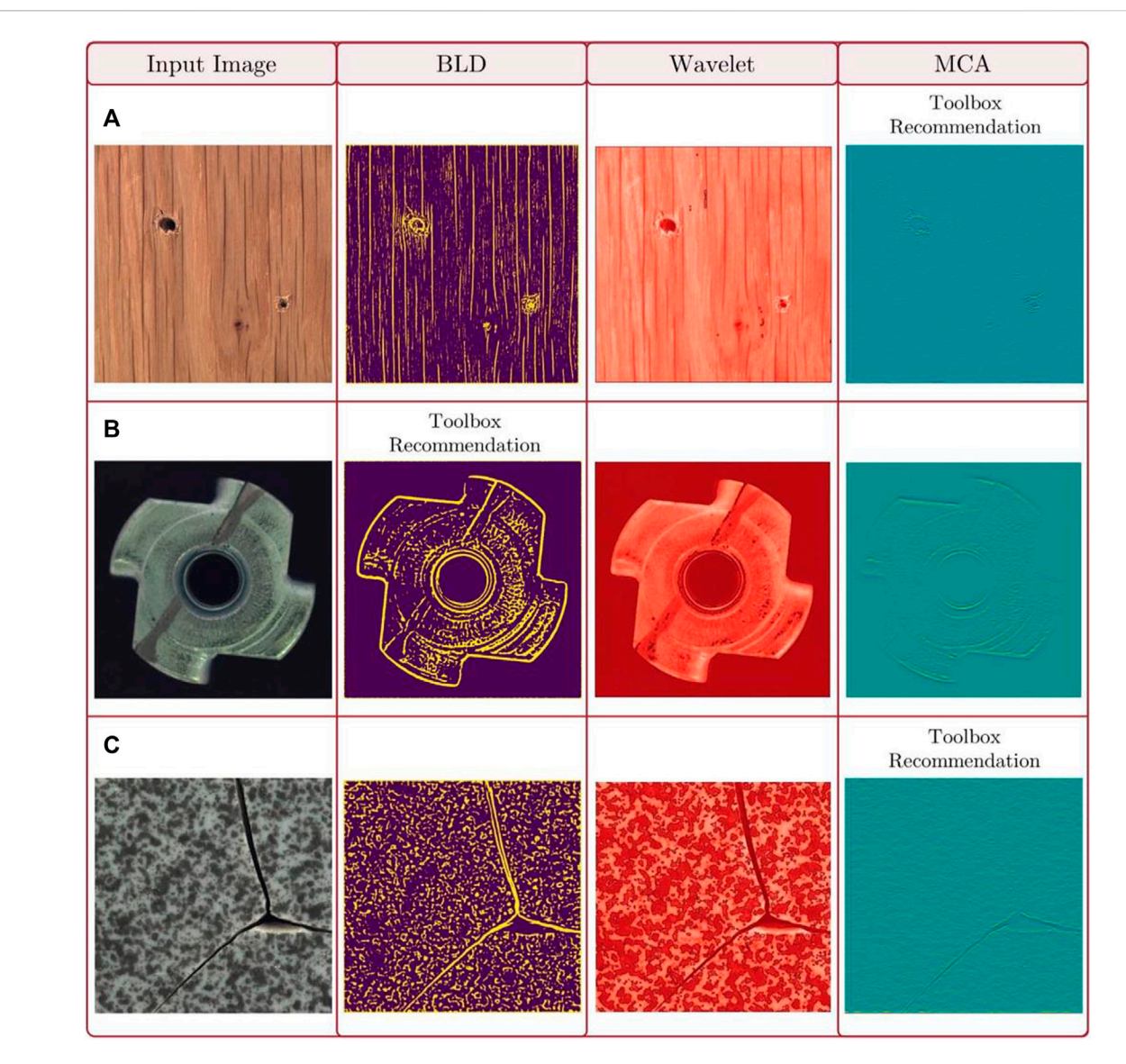


FIGURE 16
Outputs from the Toolbox for sample images from (A) Wooden (B) Metal nut and (C) Tile categories from the MVTecAD dataset (Nakkina et al., 2022).

The evaluation of various optical sensing technologies documented in the Table for the purpose of *in-situ* imaging measurements in additive manufacturing. Although not all imaging methods are discussed, the primary focus is on discussing the most prominent imaging techniques that hold substantial significance concerning high resolution in capturing process physics and their integration with ML/AI methods during model training. The objective is to examine the capabilities and performance of these technologies in a scientific context. These technologies encompass a range of methodologies and instruments that enable the non-destructive evaluation of surface characteristics during the additive manufacturing process.

In the following section, we present various case studies that employ distinct imaging methods, such as high-speed cameras, thermal cameras, and digital cameras, to monitor and analyze diverse anomalies that arise during the deposition and process mechanisms. Additionally, we explore *ex-situ* imaging methods

that integrate advanced machine learning (ML) and artificial intelligence (AI) algorithms to enhance defect detection.

3 Case studies

A practical example highlighting the contribution of *in-situ* imaging in smart manufacturing is the implementation of a smart hybrid machine tool (Optomec MTS 500), at Texas A&M University (Botcha et al., 2020). This machine tool incorporates *in-situ* imaging sensors along with other sensors, enabling the collection of data from 14 different channels. Notably, the machine is equipped with a high-speed camera capable of capturing videos at high frame rates, facilitating the observation and analysis of various process mechanisms. These mechanisms include spatter events, the emergence of powder from nozzles, and the trajectory of chips during milling operations. In an additive-

subtractive process lasting 1 hour, the high-speed camera (built: Photron Mini AX200) collects approximately 100–200 GB of data at a frame rate of 5000 FPS. Usually, this involves speed cameras are used for capturing selective segments of the process that involve process mechanisms that occur at sub-second scales. For the 1-h process, around three to four instances of such segments can be captured. High-speed cameras capture processes with exceptional temporal resolution, enabling the collection of detailed visual information.

A thermal camera (Stratonics ThermaViz System) is installed coaxially to the laser assembly, measuring temperature distributions and thermal signatures of the melt pool. The thermal camera captures data at different frame rates, typically ranging from 30 to 60 Hz. For a 1-h process, it collects around 60–120 GB of data. Other imaging systems such as optical cameras in a modern smartphone can record the entire process and generate around 20–25 GB of data if recorded at resolution of 4K at 60 FPS. These imaging devices generate big data (~200–250 GB per hour) that can be processed and analyzed using advanced analytics and machine learning algorithms.

The installation of high-resolution cameras in manufacturing machines alone does not suffice to address the challenges effectively. It is crucial to establish an appropriate data collection pipeline to ensure the value and usefulness of the collected data for subsequent analysis. Implementing a well-designed data collection pipeline is paramount as it ensures that the acquired data adheres to appropriate protocols, preventing it from inconsequential for analysis purposes (Wang et al., 2022). By collecting data with a well-defined protocol, researchers can ensure data integrity and accuracy. At Texas A&M University, a meticulous data pipeline is implemented to capture data from multiple sensors in real-time (see Figure 7), which is then stored both locally and on cloud-based storages. This dual storage approach allows for real-time monitoring of the cloud-based data and facilitates the transfer of data to other hosts for further analysis. The collected data is subject to analysis through data processing algorithms, providing opportunities to uncover hidden patterns, correlations, and insights that contribute to process optimization, quality improvement, and enhanced manufacturing performance.

In this section, we explore various case studies that pertain to the application of imaging techniques within the space of smart additive manufacturing. These imaging methods are employed to detect and identify different types of defects that may occur during manufacturing processes. Specifically, we focus on the utilization of optical sensing and intensity-based sensing methods for defect monitoring. Liu *et al.* (Liu et al., 2021) conducted a study wherein they investigated specific defects occurring in the context of DED. These defects can arise due to a combination of multiple factors. Here we discuss two primary categories of anomalies in DED process: process faults and product defect monitoring.

Process faults comprise irregularities that transpire during the deposition process itself, such as spatter events, laser focus issues (discussed in Section 3.1), and other similar occurrences. These faults can have a detrimental impact on the overall quality and integrity of the manufactured product. This detrimental impact implies negative effects or consequences that these process faults can introduce. They can result in reduced quality where the product does not meet the required standards or specifications, compromised

integrity where the structural strength of the product is weakened leading to potential failure under stress. On the other hand, product defect monitoring relates to the identification and tracking of various irregularities in the final product. This includes dimensional variations, surface waviness, morphological variations, and the detection of porosity. Monitoring these defects is crucial as they can significantly impact the functional properties and performance of the manufactured parts.

To address these challenges, optical sensing and intensity-based sensing methods have proven to be effective tools. Optical sensing techniques utilize light-based systems to capture and analyze data related to the manufacturing process. These methods enable real-time monitoring and analysis of process faults and product defects. In addition to the utilization of imaging techniques, the integration of Machine Learning (ML) and Artificial Intelligence (AI) algorithms plays a crucial role in extracting hidden information and patterns from the captured images. ML and AI techniques enable advanced analysis and interpretation of the imaging data, leading to enhanced defect detection and monitoring in smart manufacturing.

By employing ML/AI algorithms, we can train models to recognize and classify different types of defects based on the patterns and features extracted from the images. These algorithms learn from a large dataset of labeled images, allowing them to identify subtle variations and anomalies that may not be easily discernible to the human eye (discussed in Section 3.2). This capability enables automated and accurate defect detection, minimizing the reliance on manual inspection processes that can be time-consuming and prone to human error.

3.1 Process faults

In-situ monitoring plays a crucial role in the additive manufacturing process as it enables constant supervision of the process physics and facilitates the detection of anomaly events occurring during the process. The selection of accurate process parameters is paramount to avoid various defects such as porosity, dimensional inaccuracies, and surface waviness. These defects tend to have a multiplier effect, meaning that when a defect arises, it propagates through subsequent layers if not corrected. Therefore, it becomes imperative to identify the origin of defects as soon as they occur and implement corrective measures to mitigate their presence. In this context, high-speed cameras can be employed to monitor multiple process mechanisms, specifically in observing the laser focus during the printing process, spatter events, powder particle trajectory, and tracking chips mechanism in milling operation.

High-speed cameras can capture rapid events with high temporal resolution, enabling the monitoring of the laser focus during the additive manufacturing process. By recording the laser's behavior in real-time, these cameras provide valuable insights into the dynamics of the laser beam and its interaction with the printing material. Monitoring the laser focus using high-speed cameras involves capturing detailed images or videos of the laser spot during the printing process. These cameras can be synchronized with the printing system to capture images at specific time intervals or triggered by specific process events.

Through the analysis of high-speed camera footage, it becomes possible to assess the laser's focal position and evaluate its stability and consistency. Any deviations or fluctuations in the laser focus can be detected and correlated with potential defects observed in the printed part. Furthermore, the use of image processing techniques and algorithms can provide quantitative measurements of the laser spot size, shape, and intensity distribution, aiding in the identification of potential issues related to the laser focus.

Figure 8, shows a series of images obtained through the utilization of a high-speed camera during the additive manufacturing printing process. Figure 8A effectively demonstrates the laser focus at the printing track, specifically emphasizing the amalgamation of powder streams within the melt pool on the deposition track. The significance of laser focus in determining surface quality becomes apparent upon observation of these images. When the laser is appropriately focused, consecutive tracks are laid down without any observable irregularities. Conversely, when the laser deviates from its optimal focus (see Figure 8B), it becomes unfeasible to achieve a level layer. This phenomenon becomes increasingly conspicuous as the number of layers accumulates, ultimately leading to undulations in the surface. Consequently, the continuous monitoring of laser focus throughout the printing process assumes paramount importance in upholding print quality and attaining the desired surface characteristics.

Another essential capability offered by high-speed cameras is their ability to accurately detect and analyze spatter events. These spatters can have a detrimental effect on the overall quality of the built part, potentially leading to the occurrence of various defects. By employing advanced filtering techniques such as the Kalman filter, it becomes possible to effectively track and quantify the spatters in real-time as they are expelled from the melt pool.

In a study conducted by Iquebal *et al.* (Iquebal et al., 2022), it was observed that a substantial proportion of the powder material (approximately 89%) is wasted even before it enters the melt pool. Consequently, only around 11% of the powder particles successfully reaches the melt pool. Within this deposition zone, approximately 12% of the material is ejected through spattering phenomena. These spatter events involve the expulsion of molten droplets or particles from the melt pool, which can negatively impact the integrity and quality of the final build. The detection and quantification of spatters in real-time using high-speed cameras (see Figure 9), in conjunction with advanced filters like the Kalman filter, provide valuable insights into the spattering phenomenon, enabling the development of strategies to minimize its occurrence and mitigate its detrimental effects on the built part.

The utilization of pyrometer based thermal cameras in monitoring the behavior of the melt pool during the additive manufacturing printing process is witnessing a growing trend. The melt pool is a crucial phenomenon to monitor as it offers opportunities for achieving tailored properties in the manufactured components by tuning the laser power in real time. The implementation of thermal cameras enables the acquisition of comprehensive insights into the characteristics of the melt pool. Through the analysis of real-time data obtained from the thermal camera, including parameters such as peak temperature, melt pool geometry, and temperature distribution, it becomes possible to establish a closed-loop control system. By comparing the

observed parameters with the desired values, adjustments can be made to the process parameters in real-time, such as adjusting the laser power. This closed-loop control mechanism ensures that the melt pool remains within the desired temperature range and exhibits the intended geometry, leading to the desired properties in the printed component.

Furthermore, the detailed insights provided by thermal cameras allow for a deeper understanding of the melt pool behavior. By studying the temperature distribution and variations as shown in Figure 10, it becomes possible to optimize process parameters and identify potential issues that may impact the quality of the printed part. By utilizing this information, adjustments can be made to mitigate defects such as porosity, incomplete melting, or excessive heat accumulation, which can negatively impact the properties and structural integrity of the final component.

The incorporation of the Stratonics Therma Viz, installed coaxially in the Optomec MTS 500 system, enables real-time monitoring and analysis of the melt pool during the deposition process. Through the utilization of advanced algorithms, various mechanisms can be understood and quantified, leading to enhanced process control and quality assurance.

- Melt Pool Geometry: The precise measurement and characterization of the melt pool geometry are crucial for evaluating the stability and behavior of the deposition process. By capturing and analyzing real-time melt pool images, the circularity of the pool, as well as dimensions such as major and minor axis lengths, can be quantified.
- 2. Temperature Distribution: This information is critical for assessing the thermal profile and heat dissipation characteristics during the deposition process. Real-time monitoring of temperature distribution aids in identifying potential temperature variations or gradients that may affect the material's solidification behavior, resulting in defects such as porosity, cracking, or incomplete fusion.
- 3. Thermal Gradients: The algorithms integrated with the thermal camera enable the calculation of thermal gradients within the melt pool as shown in Figure 11. Thermal gradients represent the rate of temperature change across the material. Monitoring these gradients in real-time provides valuable information on heat transfer phenomena, including cooling rates and heat dissipation patterns. Ripple phenomena, observed in DED processes, are often influenced by thermal gradients, alloying effects, and recoil pressure. By quantifying thermal gradients, the dynamics of ripple formation (Balhara et al., 2023) and its correlation with process parameters can be analyzed, contributing to improved process optimization and defect detection.

Optical cameras have provided an excellent means of *in-situ* monitoring due to their convenience, affordability, and accessibility for a long time. The advancement in the smartphone industry has made it even more convenient given the instrumentation of these modern smartphones with high-tech sophisticated optical cameras with easy-to-use interfaces and the form factor. Smartphones can capture high resolution videos or images during manufacturing giving a great overall picture of the process. This translates to a foundation for operators to visually inspect the process, identify any

artifacts of interest, and monitor several metrics associated with the process.

By using appropriate filters or image post-processing techniques, smartphones are even capable of capturing the thermal history of the process. This thermal monitoring allows for the identification of abnormal heating or cooling patterns in the process. By strategically positioning the smartphone camera, operators can capture close-up images and videos of the process. Moreover, there are a lot of computer vision techniques that can be used to further analyze the images or videos, opening a possibility for analyses such as object detection and tracking. *In-situ* monitoring using smartphone cameras (see Figure 12) can also allow for process optimization by extracting valuable data in the form of adjustable and refinable process parameters for the operators. Over time, this iterative feedback assists in improving the overall process in terms of quality and efficiency.

3.2 Product defects

Defects in manufacturing manifest in varied forms and attributes which add to the woes of developing one-shot detection methodologies, while it is also expensive to generate a dataset of images capturing the variety to train these models. Therefore, many image processing techniques have been implemented that specialize in detecting certain defects due to the surface's nature. Indeed, while *in-situ* imaging techniques offer numerous advantages, post-process imaging techniques are equally, and sometimes more, important for analyzing specific properties of manufactured components. Advanced imaging methods, such as 3D optical profilometry, Scanning Electron Microscopy (SEM), and Energy Dispersive Spectroscopy (EDS), play a significant role in providing high-resolution images suitable for detailed analysis.

Post-process imaging techniques enable the examination of manufactured components at a higher level of magnification and resolution, facilitating the inspection of fine details and surface characteristics. 3D optical profilometry, for instance, allows for the precise measurement of surface profiles, enabling the evaluation of dimensional accuracy, surface roughness, and features at a microscale level. Scanning Electron Microscopy (SEM) provides exceptional imaging capabilities with high-resolution and magnification. It allows for the observation of surface morphology, microstructure, and topographical features at nanoscale levels (see Figure 13A). SEM coupled with EDS provides valuable elemental analysis, enabling the identification and mapping of different chemical elements present in the sample.

Recent advancements in machine learning and artificial intelligence have further enhanced post-process imaging techniques. These technologies enable defect localization and analysis based on imaging data. Machine learning algorithms can be trained to detect and classify various types of defects, aiding in quality control and process optimization.

The utilization of big data in post-process imaging techniques offers significant contributions to the field. It enables efficient collection, storage, and management of large-scale imaging datasets, while advanced analytics techniques facilitate automated feature extraction, defect detection, and classification. Integration

with other data sources allows for a comprehensive analysis of the manufacturing process, while predictive analytics models based on historical imaging data assist in forecasting potential defects. Real-time monitoring and feedback are facilitated through the streaming and processing of data, enabling timely intervention and corrective actions. Furthermore, big data technologies provide tools for data visualization and reporting, aiding in the interpretation and communication of findings.

Pores and voids in DED processes exhibit a stochastic formation pattern as they emerge from multiple physical mechanisms over multiple sizes (ranging 10^{-5} – 10^{-3} m), and at diverse locations including the surface, sub-surface or between deposited layers (see Figure 13C). Digital images and optical micrographs can be used to characterize surface porosity that manifest as a result of various mechanisms such as (a) micro-void formations caused due to insufficient overlap and fusion between adjacent printing tracks, and (b) pore formation due to the spatter events during the DED process.

In the past decade, deep learning models have been widely used in the manufacturing sector for real-time process monitoring and anomaly detection, leveraging multimodal sensor data. However, the complex, non-linear nature of these models often results in a lack of transparency, making it difficult to interpret their predictions and thereby reducing trust in the model. In response to this challenge, there has been a significant shift towards the use of Explainable AI (XAI) techniques, which aim to increase the interpretability and transparency of AI models. XAI techniques along with thermal images of the melt pool proved to better understand the lasermaterial interactions and discover the nature of spatter events that result in the occurrence of porosity in localized surface elements (Karthikeyan et al., 2023). Recently, Karthikeyan et al. (Karthikeyan et al., 2022) developed an approach that integrates explainable AI (XAI) into ultrasound imaging for rapid detection of artifacts, including product defects, in 3D printed components. Leveraging ultrasound imaging offers a non-destructive means of inspecting the internal structure of 3D printed parts, particularly useful for identifying defects that are not visible on the surface. The incorporation of XAI into this process serves to validate AIdriven decisions, providing decision-makers with an enhanced transparency into the discernible features within the images that contribute to defect classification.

Although advanced machine learning techniques have been employed to analyze manufacturing data and enhance production strategies, the challenge of labeling data for supervised learning methods remains a significant obstacle. Defects in manufacturing exhibit diverse forms and characteristics, complicating the development of one-shot detection methodologies. Furthermore, the generation of an extensive dataset encompassing the various defect types for model training purposes can be prohibitively costly. Consequently, numerous specialized image processing techniques have been implemented to address this issue, focusing on the detection of specific defects based on the surface properties.

With the emergence of Manufacturing-as-a-Service (MaaS) paradigm, it becomes imperative to secure essential products against counterfeiting and cyber-attacks (Tiwari et al., 2021). Anticounterfeit tags, such as QR codes introduced on the surface of physical products can be tampered with, thus destroying the ability to identify these parts. Hence, in order to introduce

anticounterfeit tags inside the physical product, the 3D printed parts were embedded with spherical markers of diameter 0.48 mm (see Figure 13F). The markers were dispersed at both shallow (1–3 mm depth) and deeper (9–12 mm depth) locations, emulating the occurrence of defects (e.g., internal pores and voids) and embedded authentication codes in a product. The authors employed a fast-scanning ultrasound imaging technique coupled with a convolutional deep learning software framework to obtain speed and accuracy in scanning the internal markers present inside 3D printed parts. They were able to accurately detect the internal markers at different locations within the product to accuracies exceeding 80%.

In Iquebal et al. (Iquebal and Bukkapatnam, 2022), the authors propose a fully unsupervised segmentation approach using a continuous max-flow formulation over the image domain while optimally estimating the flow parameters from the image characteristics. Image segmentation approaches based on the energy minimization framework, particularly graph-based methods, offer an elegant means to segment images without extensive training. The framework is based on iteratively estimating the image labels by solving the maxflow problem while optimally estimating the flow capacities from the image characteristics. The segmentation problem is set up as a maximum posteriori estimation (MAP) of the image labels and shows that it is equivalent to solving the max-flow problem given the flow capacities are known. By using the current optimum of the max-flow problem, the flow capacities are estimated by employing a Markov random field (MRF) prior over the flow capacities. For a detailed understanding of the framework and algorithm, we direct the readers to their paper (Iquebal and Bukkapatnam, 2022).

The current case study presents the segmentation capabilities of the above-mentioned framework for common defects on additively manufactured surfaces, namely, balling effect, and porosity. Figure 14A and Figure 15A show the representative surface from two samples that were additively manufactured. Figures 14B–F, Figures 15B–F give the comparative results from different segmentation algorithms, namely-means with 2 clusters, Gaussian mixture model with expectation maximization, spatially constrained Gaussian mixture model with k-means initialization (Nguyen and Wu, 2013), mean shift (Comaniciu and Meer, 2002), and Unsupervised min cut (Iquebal and Bukkapatnam, 2022).

Numerous studies have proposed various techniques in image processing, machine learning, and neural network models to address defect detection and segmentation in specific defect domains. However, the diverse nature and characteristics of defects in manufacturing pose challenges in developing comprehensive one-shot detection methods. Furthermore, creating a dataset encompassing the wide range of defect variations is costly when training a one-shot machine learning model. Nakkina *et al.* (Nakkina *et al.*, 2022) introduces a framework that comprises three mind-maps aimed at capturing the fundamental aspects of defect detection.

The first mind-map proposes a classification system for manufacturing defects based on their visual attributes. The objective of the second mind-map is to identify relevant image processing methodologies including thresholding, Fourier analysis, line detection, neural networks, and more. The third mapping aims to establish connections between specific defect classes and

corresponding image processing techniques. These three mindmaps collectively serve as a foundation for developing or adapting defect detection approaches tailored to specific use cases. Additionally, the authors introduce an empirical recommendation formula utilizing three image metrics: entropy, universal Quality Index (UQI), and Rosenberger's. This formula facilitates the evaluation of method performance across a given class of images. Nakkina *et al.* (Nakkina et al., 2022) showcases the implementation of a Smart Defect Segmentation Toolbox assimilating methodologies like Wavelet Analysis, Morphological Component Analysis (MCA), Basic Line Detector (BLD) and presents case studies to support the working of the recommendation formula.

$$Score = \left(\frac{1}{2}Rosenberger's\right) + \left(\frac{1}{4}UQI\right) - \left(\frac{1}{4}Entropy\right)$$

The MVTecAD dataset identifies industrial inspection tasks as the ideal scenarios introducing a comprehensive dataset for unsupervised anomaly detection (Bergmann et al., 2019). Figure 16 tabulates the findings of the toolbox when tested on three sample images from a wooden, metal nut, and tile categories from the MVTecAD dataset respectively. The recommendations based on the formula given by the toolbox for defect detection in each of these cases are also mentioned.

4 Conclusions and future work

This chapter delves into the rapidly increasing significance of advanced imaging techniques, specifically in the domain of fusion-based additive manufacturing. Optical cameras, thermal cameras, and via high-speed cameras can enable real-time monitoring, facilitating prompt defect detection, deviations from standard operating procedures, or any anomalous behavior. Thereby, timely intervention is possible which can lead to improved product quality, reduction in downtime, and improved uptime and productivity. Such monitoring also allows for a deeper understanding of the underlying physics involved in the manufacturing process, offering neat opportunities for process optimization. Key takeaways from the chapter are listed as follows.

- High-speed imaging demonstrates its efficacy in capturing spatter particles expelled from the melt pool during the additive manufacturing process. The real-time detection and quantification of spatters using high-speed cameras, combined with advanced filtering techniques like the Kalman filter, offer valuable insights into the spattering phenomenon. This information can then be leveraged to implement closed-loop control strategies within the manufacturing system. Furthermore, the high-speed imaging technique proves effective in identifying deviations in the laser focus, such as when it moves away from the intended printing track. This timely identification enables prompt optimization of process parameters to mitigate defects such as dimensional inaccuracies and surface waviness.
- The thermal camera exhibits its capability to monitor key characteristics of the melt pool, including peak temperature and melt pool geometry during additive manufacturing

processes. Deviations from the standard characteristics serve as indicative signatures for optimizing process parameters. Real-time analysis of thermal data allows for the assessment of heat distribution and thermal gradients within the melt pool, providing insights for the implementation of closed-loop control strategies. By adjusting the laser power in real-time based on the observed thermal information, tailored properties of the components can be achieved.

- Digital cameras integrated into smartphones offer a practical solution for recording the complete manufacturing process.
 The captured data from these cameras can subsequently be utilized to synchronize and align the multi-modal sensor data collected during the process. Leveraging the capabilities of smartphone cameras in this manner provides a cost-effective and accessible means to enhance data fusion and analysis in smart manufacturing.
- Ex-situ imaging methods, when combined with the integration of machine learning/artificial intelligence (ML/AI) techniques, offer the opportunity to analyze data with enhanced depth and sophistication. The high-resolution images captured via ex-situ imaging systems serve as excellent inputs to state-of-theart deep learning models for a variety of applications.

Given the remarkable progress and use of advanced imaging technology in smart manufacturing, there is potential for future research work in several avenues. One such area involves integration of the imaging data with advanced ML/AI methodologies. Another aspect lies in the use of multimodal nature of data. Given the plethora of imaging options, most manufacturers employ more than one at the same time to monitor their process. Multimodal data fusion that incorporates diverse types of image-based data is a blooming area of research, especially in healthcare and wearable devices industry. By fusing data from optical, thermal, high-speed, and other types of cameras with exsitu imaging, researchers can extract synergistic information to have a more holistic understanding of the process. Another challenge lies in the fact that the data resulting from such advanced imaging techniques is usually large and can sometimes slow down real-time processing and analyses. Developing data pipelines that provide capabilities for realtime processing of such data without any latency issues or lag is essential for immediate decision-making in such scenarios. To further optimize the processes, creation of seamless and datadriven ecosystem comprised of integrated imaging technologies and IoT sensors is preferred. A common disadvantage that is being tackled is the heavy cost expense that comes from some of these imaging systems. Developing cost-effective yet reliable imaging technologies will lead to widespread adoption in the

industry, especially for small- and medium-sized enterprises. By lowering the entry barriers and easy-to-use interfaces of such imaging systems will democratize access to advanced capabilities, empowering a broader range of industries.

Data availability statement

The original contributions presented in the study are included in the article/Supplementary material, further inquiries can be directed to the corresponding author.

Author contributions

HB: Data curation, Formal Analysis, Investigation, Methodology, Writing-original draft. AK: Data curation, Formal Analysis, Writing-review and editing. AH: Data curation, Formal Analysis, Writing-review and editing. TN: Data curation, Formal Analysis, Writing-review and editing. SB: Conceptualization, Funding acquisition, Project administration, Resources, Supervision, Writing-review and editing.

Funding

The author(s) declare financial support was received for the research, authorship, and/or publication of this article. This work was supported by the Rockwell International Professorship, Texas A&M University XGrants and National Science Foundation (S&AS grant award #1849085 and ECCS 1953694).

Conflict of interest

The authors declare that the research was conducted in the absence of any commercial or financial relationships that could be construed as a potential conflict of interest.

Publisher's note

All claims expressed in this article are solely those of the authors and do not necessarily represent those of their affiliated organizations, or those of the publisher, the editors and the reviewers. Any product that may be evaluated in this article, or claim that may be made by its manufacturer, is not guaranteed or endorsed by the publisher.

References

Abhilash, P. M., and Ahmed, A. (2023). An image-processing approach for polishing metal additive manufactured components to improve the dimensional accuracy and surface integrity. *Int. J. Adv. Manuf. Technol.* 125 (7), 3363–3383. doi:10.1007/s00170-023-10916-1

Akbari, M., and Kovacevic, R. (2019). Closed loop control of melt pool width in robotized laser powder–directed energy deposition process. *Int. J. Adv. Manuf. Technol.* 104 (5–8), 2887–2898. doi:10.1007/s00170-019-04195-y

Ali, N., Tomesani, L., Ascari, A., and Fortunato, A. (2022). Fabrication of thin walls with and without close loop control as a function of scan Strategy via direct energy deposition. *Lasers Manuf. Mater. Process.* 9 (1), 81–101. doi:10.1007/s40516-022-00164-8

Allam, A., Alfahmi, O., Patel, H., Sugino, C., Harding, M., Ruzzene, M., et al. (2022). Ultrasonic testing of thick and thin Inconel 625 alloys manufactured by laser powder bed fusion. *Ultrasonics* 125, 106780. doi:10.1016/j.ultras.2022.106780

Andani, M. T., Dehghani, R., Karamooz-Ravari, M. R., Mirzaeifar, R., and Ni, J. (2017). Spatter formation in selective laser melting process using multi-laser technology. *Mater. Des.* 131, 460–469. doi:10.1016/j.matdes.2017.06.040

- Arnold, C., and Körner, C. (2021). Electron-optical *in-situ* metrology for electron beam powder bed fusion: calibration and validation. *Meas. Sci. Technol.* 33 (1), 014001. doi:10.1088/1361-6501/ac2d5c
- Bakre, C., Meyer, T., Jamieson, C., Nassar, A. R., Reutzel, E. W., and Lissenden, C. J. (2022). *In-situ* laser ultrasound-based Rayleigh wave process monitoring of DED-AM metals. *Res. Nondestruct. Eval.* 33 (4–5), 218–242. doi:10.1080/09349847.2022.2120652
- Balhara, H., Botcha, B., Wolff, S. J., and Bukkapatnam, S. T. S. (2023). Ripple formations determine the heterogeneous microstructure of directed energy deposition (DED)-printed 316L components. *Mater. Des.* 227, 111756. doi:10.1016/j. matdes.2023.111756
- Barrett, C., Carradero, C., Harris, E., Rogers, K., MacDonald, E., and Conner, B. (2019). Statistical analysis of spatter velocity with high-speed stereovision in laser powder bed fusion. *Prog. Addit. Manuf.* 4 (4), 423–430. doi:10.1007/s40964-019-00094-6
- Barrett, C., Carradero, C., Harris, E., McKnight, J., Walker, J., MacDonald, E., et al. (2018a). "Low cost, high speed stereovision for spatter tracking in laser powder bed fusion," in 2018 International Solid Freeform Fabrication Symposium (Austin: University of Texas at Austin).
- Barrett, C., MacDonald, E., Conner, B., and Persi, F. (2018b). Micron-level layer-wise surface profilometry to detect porosity defects in powder bed fusion of Inconel 718. *JOM* 70 (9), 1844–1852. doi:10.1007/s11837-018-3025-7
- Becker, D., Boley, S., Eisseler, R., Stehle, T., Möhring, H. C., Onuseit, V., et al. (2021). Influence of a closed-loop controlled laser metal wire deposition process of S Al 5356 on the quality of manufactured parts before and after subsequent machining. *Prod. Eng. Res. Devel.* 15 (3–4), 489–507. doi:10.1007/s11740-021-01030-w
- Bergmann, P., Fauser, M., Sattlegger, D., and Steger, C. (2019). "MVTec ad -- A comprehensive real-world dataset for unsupervised anomaly detection," in presented at the Proceedings of the IEEE/CVF Conference on Computer Vision and Pattern Recognition, 9592–9600. Accessed: Jul. 14, 2023.
- Bernauer, C., Zapata, A., and Zaeh, M. F. (2022a). Toward defect-free components in laser metal deposition with coaxial wire feeding through closed-loop control of the melt pool temperature. *J. Laser Appl.* 34 (4), 042044. doi:10.2351/7.0000773
- Bernauer, C. J., Zapata, A., Kick, L., Weiss, T., Sigl, M. E., and Zaeh, M. F. (2022b). Pyrometry-based closed-loop control of the melt pool temperature in Laser Metal Deposition with coaxial wire feeding. *Procedia CIRP* 111, 296–301. doi:10.1016/j.procir. 2022.08.025
- Bidare, P., Maier, R. R. J., Beck, R. J., Shephard, J. D., and Moore, A. J. (2017). An open-architecture metal powder bed fusion system for *in-situ* process measurements. *Addit. Manuf.* 16, 177–185. doi:10.1016/j.addma.2017.06.007
- Black, D., Henderson, J., Klocke, P., Shumway, L., and Crane, N. B. (2023). Dark field optical observation of polymer powder bed fusion for process monitoring and control. *Addit. Manuf.* 74, 103715. doi:10.1016/j.addma.2023.103715
- Boschetto, A., Bottini, L., and Vatanparast, S. (2023). Powder bed monitoring via digital image analysis in additive manufacturing. *J. Intell. Manuf.* doi:10.1007/s10845-023-02001-7
- Boschetto, A., Bottini, L., Vatanparast, S., and Veniali, F. (2022). Part defects identification in selective laser melting via digital image processing of powder bed anomalies. *Prod. Eng. Res. Devel.* 16 (5), 691–704. doi:10.1007/s11740-022-01112-3
- Botcha, B., Iquebal, A. S., and Bukkapatnam, S. T. S. (2020). Smart manufacturing multiplex. *Manuf. Lett.* 25, 102–106. doi:10.1016/j.mfglet.2020.08.004
- Bugatti, M., and Colosimo, B. M. (2022). Towards real-time *in-situ* monitoring of hotspot defects in L-PBF: a new classification-based method for fast video-imaging data analysis. *J. Intell. Manuf.* 33 (1), 293–309. doi:10.1007/s10845-021-01787-y
- Chabot, A., Laroche, N., Carcreff, E., Rauch, M., and Hascoët, J.-Y. (2020). Towards defect monitoring for metallic additive manufacturing components using phased array ultrasonic testing. *J. Intell. Manuf.* 31 (5), 1191–1201. doi:10.1007/s10845-019-01505-9
- Chebil, G., Bettebghor, D., Renollet, Y., Lapouge, P., Davoine, C., Thomas, M., et al. (2023). Deep learning object detection for optical monitoring of spatters in L-PBF. *J. Mater. Process. Technol.* 319, 118063. doi:10.1016/j.jmatprotec.2023.118063
- Chechik, L., Goodall, A. D., Christofidou, K. A., and Todd, I. (2023). Controlling grain structure in metallic additive manufacturing using a versatile, inexpensive process control system. *Sci. Rep.* 13 (1), 10003. doi:10.1038/s41598-023-37089-x
- Chen, L., Yao, X., Chew, Y., Weng, F., Moon, S. K., and Bi, G. (2020). Data-driven adaptive control for laser-based additive manufacturing with automatic controller tuning. *Appl. Sci.* 10 (22), 7967. doi:10.3390/app10227967
- Cherif, L., Safdar, M., Lamouche, G., Wanjara, P., Paul, P., Wood, G., et al. (2023). Evaluation of key spatiotemporal learners for print track anomaly classification using melt pool image streams. doi:10.48550/arXiv.2308.14861
- Comaniciu, D., and Meer, P. (2002). Mean shift: a robust approach toward feature space analysis. *IEEE Trans. Pattern Analysis Mach. Intell.* 24 (5), 603–619. doi:10.1109/34.1000236

D'Accardi, E., Chiappini, F., Giannasi, A., Guerrini, M., Maggiani, G., Palumbo, D., et al. (2023). Online monitoring of direct laser metal deposition process by means of infrared thermography. *Prog. Addit. Manuf.* doi:10.1007/s40964-023-00496-7

- Davis, G., Nagarajah, R., Palanisamy, S., Rashid, R. A. R., Rajagopal, P., and Balasubramaniam, K. (2019). Laser ultrasonic inspection of additive manufactured components. *Int. J. Adv. Manuf. Technol.* 102 (5), 2571–2579. doi:10.1007/s00170-018-3046-v
- De Groot, P. J. (2019). A review of selected topics in interferometric optical metrology. *Rep. Prog. Phys.* 82 (5), 056101. doi:10.1088/1361-6633/ab092d
- Delacroix, T., Lomello, F., Schuster, F., Maskrot, H., Jacquier, V., Lapouge, P., et al. (2023). Measurement of powder bed oxygen content by image analysis in laser powder bed fusion. *Mater. Des.* 226, 111667. doi:10.1016/j.matdes.2023.111667
- DePond, P. J., Guss, G., Ly, S., Calta, N. P., Deane, D., Khairallah, S., et al. (2018). *In situ* measurements of layer roughness during laser powder bed fusion additive manufacturing using low coherence scanning interferometry. *Mater. Des.* 154, 347–359. doi:10.1016/j.matdes.2018.05.050
- el Farsy, A., Tighidet, E. C., Ballage, C., and Minea, T. (2023). Spatiotemporal characterization of evaporated atoms during electron beam melting additive manufacturing by advanced laser diagnostics. *J. Appl. Phys.* 133 (4), 044901. doi:10. 1063/5.0131102
- Eschner, E., Staudt, T., and Schmidt, M. (2020). Correlation of spatter behavior and process zone formation in powder bed fusion of metals. *CIRP Ann.* 69 (1), 209–212. doi:10.1016/j.cirp.2020.04.092
- Farshidianfar, M. H., Khajepour, A., and Gerlich, A. (2016). Real-time control of microstructure in laser additive manufacturing. *Int. J. Adv. Manuf. Technol.* 82 (5–8), 1173–1186. doi:10.1007/s00170-015-7423-5
- Farshidianfar, M. H., Khodabakhshi, F., Khajepour, A., and Gerlich, A. P. (2021a). Closed-loop control of microstructure and mechanical properties in additive manufacturing by directed energy deposition. *Mater. Sci. Eng. A* 803, 140483. doi:10.1016/j.msea.2020.140483
- Farshidianfar, M. H., Khodabakhshi, F., Khajepour, A., and Gerlich, A. P. (2021b). Closed-loop deposition of martensitic stainless steel during laser additive manufacturing to control microstructure and mechanical properties. *Opt. Lasers Eng.* 145, 106680. doi:10.1016/j.optlaseng.2021.106680
- Fischer, F. G., Birk, N., Rooney, L., Jauer, L., and Schleifenbaum, J. H. (2021). Optical process monitoring in Laser Powder Bed Fusion using a recoater-based line camera. *Addit. Manuf.* 47, 102218. doi:10.1016/j.addma.2021.102218
- Freeman, F., Chechik, L., Thomas, B., and Todd, I. (2023). Calibrated closed-loop control to reduce the effect of geometry on mechanical behaviour in directed energy deposition. *J. Mater. Process. Technol.* 311, 117823. doi:10.1016/j.jmatprotec.2022. 117823
- Fu, S., Kor, W. S., Cheng, F., and Seah, L. K. (2020). *In-situ* measurement of surface roughness using chromatic confocal sensor. *Procedia CIRP* 94, 780–784. doi:10.1016/j. procir.2020.09.133
- Gardfjell, M., Reith, M., Franke, M., and Körner, C. (2023). *In situ* inclusion detection and material characterization in an electron beam powder bed fusion process using electron optical imaging. *Materials* 16 (12), 4220. Art. no. 12. doi:10. 3390/ma16124220
- Gibson, B. T., Bandari, Y., Richardson, B., Henry, W., Vetland, E., Sundermann, T., et al. (2020). Melt pool size control through multiple closed-loop modalities in laser-wire directed energy deposition of Ti-6Al-4V. *Addit. Manuf.* 32, 100993. doi:10.1016/j. addma.2019.100993
- Gibson, B. T., Richardson, B. S., Sundermann, T. W., and Love, L. J. (2019). Beyond the toolpath: site-specific melt pool size control enables printing of extra-toolpath geometry in laser wire-based directed energy deposition. *Appl. Sci.* 9 (20), 4355. doi:10. 3390/app9204355
- Giusti, A., Dotta, M., Maradia, U., Boccadoro, M., Gambardella, L. M., and Nasciuti, A. (2020). Image-based measurement of material roughness using machine learning techniques. *Procedia CIRP* 95, 377–382. doi:10.1016/j.procir.2020.02.292
- Gobert, C., Reutzel, E. W., Petrich, J., Nassar, A. R., and Phoha, S. (2018). Application of supervised machine learning for defect detection during metallic powder bed fusion additive manufacturing using high resolution imaging. *Addit. Manuf.* 21, 517–528. doi:10.1016/j.addma.2018.04.005
- Gomez, C., Su, R., De Groot, P., and Leach, R. (2020). Noise reduction in coherence scanning interferometry for surface topography measurement. *Nanomanufacturing Metrology* 3 (1), 68–76. doi:10.1007/s41871-020-00057-4
- Grasso, M. (2021). In situ monitoring of powder bed fusion homogeneity in electron beam melting. Materials 14 (22), 7015. Art. no. 22. doi:10.3390/ma14227015
- Guerra, M. G., Errico, V., Fusco, A., Lavecchia, F., Campanelli, S. L., and Galantucci, L. M. (2022). High resolution-optical tomography for in-process layerwise monitoring of a laser-powder bed fusion technology. *Addit. Manuf.* 55, 102850. doi:10.1016/j.addma. 2022.102850
- Harshavardhan, A., Venugopal, T., and Babu, S. (2018). "3D surface measurement through easy-snap phase shift fringe projection," in *Progress in advanced computing and intelligent engineering* (Cham: Springer), 179–186.

Hirsch, M., Catchpole-Smith, S., Patel, R., Marrow, P., Li, W., Tuck, C., et al. (2017). Meso-scale defect evaluation of selective laser melting using spatially resolved acoustic spectroscopy. *Proc. R. Soc. A Math. Phys. Eng. Sci.* 473 (2205), 20170194. doi:10.1098/rspa.2017.0194

- Hirsch, M., Dryburgh, P., Catchpole-Smith, S., Patel, R., Parry, L., Sharples, S., et al. (2018). Targeted rework strategies for powder bed additive manufacture. *Addit. Manuf.* 19, 127–133. doi:10.1016/j.addma.2017.11.011
- Honarvar, F., Patel, S., Vlasea, M., Amini, H., and Varvani-Farahani, A. (2021). Nondestructive characterization of laser powder bed fusion components using high-frequency phased array ultrasonic testing. *J. Materi Eng Perform* 30 (9), 6766–6776. doi:10.1007/s11665-021-05988-7
- Hu, D., and Kovacevic, R. (2003a). Modelling and measuring the thermal behaviour of the molten pool in closed-loop controlled laser-based additive manufacturing. *Proc. Institution Mech. Eng. Part B J. Eng. Manuf.* 217 (4), 441–452. doi:10.1243/095440503321628125
- Hu, D., and Kovacevic, R. (2003b). Sensing, modeling and control for laser-based additive manufacturing. *Int. J. Mach. Tools Manuf.* 43 (1), 51–60. doi:10.1016/S0890-6955(02)00163-3
- Huang, C., Wang, G., Song, H., Li, R., and Zhang, H. (2022). Rapid surface defects detection in wire and arc additive manufacturing based on laser profilometer. *Measurement* 189, 110503. doi:10.1016/j.measurement.2021.110503
- Iquebal, A. S., Botcha, B., and Bukkapatnam, S. (2020). Towards rapid, *in situ* characterization for materials-on-demand manufacturing. *Manuf. Lett.* 23, 29–33. doi:10.1016/j.mfglet.2019.11.002
- Iquebal, A. S., and Bukkapatnam, S. (2022). Consistent estimation of the max-flow problem: towards unsupervised image segmentation. *IEEE Trans. Pattern Analysis Mach. Intell.* 44 (5), 2346–2357. doi:10.1109/TPAMI.2020.3039745
- Iquebal, A. S., Yadav, A., Botcha, B., Krishna Gorthi, R., and Bukkapatnam, S. (2022). Tracking and quantifying spatter characteristics in a laser directed energy deposition process using Kalman filter. *Manuf. Lett.* 33, 692–700. doi:10.1016/j. mfglet.2022.07.086
- Iravani-Tabrizipour, M., and Toyserkani, E. (2007). An image-based feature tracking algorithm for real-time measurement of clad height. *Mach. Vis. Appl.* 18 (6), 343–354. doi:10.1007/s00138-006-0066-7
- Jiang, Z., Zhang, A., Chen, Z., Ma, C., Yuan, Z., Deng, Y., et al. (2023). A deep convolutional network combining layerwise images and defect parameter vectors for laser powder bed fusion process anomalies classification. *J. Intell. Manuf.* doi:10.1007/s10845-023-02183-4
- Kanatani, K., Sugaya, Y., and Niitsuma, H. (2008). Triangulation from two views revisited: hartley-Sturm vs. optimal correction. *practice* 4 (5).
- Kanko, J. A., Sibley, A. P., and Fraser, J. M. (2016). *In situ* morphology-based defect detection of selective laser melting through inline coherent imaging. *J. Mater. Process. Technol.* 231, 488–500. doi:10.1016/j.jmatprotec.2015.12.024
- Karthikeyan, A., Balhara, H., Lianos, A. K., Hanchate, A., and Bukkapatnam, S. T. (2023). *In-situ* surface porosity prediction in DED (directed energy deposition) printed SS316L parts using multimodal sensor fusion. arXiv Available at: https://arxiv.org/abs/2304.08658.
- Karthikeyan, A., Tiwari, A., Zhong, Y., and Bukkapatnam, S. T. S. (2022). Explainable AI-infused ultrasonic inspection for internal defect detection. *CIRP Ann.* 71 (1), 449–452. doi:10.1016/j.cirp.2022.04.036
- Kumar, M., and Garg, D. P. (2004). "Intelligent multi-sensor fusion techniques in flexible manufacturing workcells," in presented at the Proceedings of the 2004 American Control Conference, Boston, MA, USA, 30 June 2004 02 July 2004 (IEEE), 5375–5380.
- Lapointe, S., Guss, G., Reese, Z., Strantza, M., Matthews, M. J., and Druzgalski, C. L. (2022). Photodiode-based machine learning for optimization of laser powder bed fusion parameters in complex geometries. *Addit. Manuf.* 53, 102687. doi:10.1016/j.addma. 2022.102687
- Lazaros, N., Sirakoulis, G. C., and Gasteratos, A. (2008). Review of stereo vision algorithms: from software to hardware. *Int. J. Optomechatronics* 2 (4), 435–462. doi:10. 1080/15599610802438680
- Leung, C. L. A., Marussi, S., Atwood, R. C., Towrie, M., Withers, P. J., and Lee, P. D. (2018). *In situ* X-ray imaging of defect and molten pool dynamics in laser additive manufacturing. *Nat. Commun.* 9 (1), 1355. Art. no. 1. doi:10.1038/s41467-018-03734-7
- Li, J., Zheng, Y., Liu, L., and Li, B. (2021a). 4D line-scan hyperspectral imaging. *Opt. Express* 29 (21), 34835–34849. doi:10.1364/oe.441213
- Li, Y., Li, X., Zhang, G., Horváth, I., and Han, Q. (2021b). Interlayer closed-loop control of forming geometries for wire and arc additive manufacturing based on fuzzy-logic inference. *J. Manuf. Process.* 63, 35–47. doi:10.1016/j.jmapro.2020.04.009
- Liang, Z., Chang, B., Zhang, H., Li, Z., Peng, G., Du, D., et al. (2022). Electric current evaluation for process monitoring in electron beam directed energy deposition. *Int. J. Mach. Tools Manuf.* 176, 103883. doi:10.1016/j.ijmachtools.2022.103883
- Liang, Z., Liao, Z., Zhang, H., Li, Z., Wang, L., Chang, B., et al. (2023). Improving process stability of electron beam directed energy deposition by closed-loop control of molten pool. *Addit. Manuf.* 72, 103638. doi:10.1016/j.addma.2023.103638

- Liao, S., Webster, S., Huang, D., Council, R., Ehmann, K., and Cao, J. (2022). Simulation-guided variable laser power design for melt pool depth control in directed energy deposition. *Addit. Manuf.* 56, 102912. doi:10.1016/j.addma.2022. 102912
- Lin, X., Wang, Q., Fuh, J. Y. H., and Zhu, K. (2022). Motion feature based melt pool monitoring for selective laser melting process. *J. Mater. Process. Technol.* 303, 117523. doi:10.1016/j.jmatprotec.2022.117523
- Liu, C., Wang, R., Kong, Z., Babu, S., Joslin, C., and Ferguson, J. (2019). "Real-time 3D surface measurement in additive manufacturing using deep learning," in presented at the 2019 International Solid Freeform Fabrication Symposium (University of Texas at Austin)
- Liu, M., Kumar, A., Bukkapatnam, S., and Kuttolamadom, M. (2021). A review of the anomalies in directed energy deposition (DED) processes & potential solutions Part Quality & defects. *Procedia Manuf.* 53, 507–518. doi:10.1016/j.promfg.2021. 06.093
- Liu, P., Yang, L., Yi, K., Kundu, T., and Sohn, H. (2023). Application of nonlinear ultrasonic analysis for *in situ* monitoring of metal additive manufacturing. *Struct. Health Monit.* 22 (3), 1760–1775. doi:10.1177/14759217221113447
- Liu, R., Wang, Z., Sparks, T., Liou, F., and Nedic, C. (2017). Stereo vision-based repair of metallic components. *Rapid Prototyp. J.* 23 (1), 65–73. doi:10.1108/RPJ-09-2015-0118
- Liu, T., Lough, C. S., Sehhat, H., Ren, Y. M., Christofides, P. D., Kinzel, E. C., et al. (2022). *In-situ* infrared thermographic inspection for local powder layer thickness measurement in laser powder bed fusion. *Addit. Manuf.* 55, 102873. doi:10.1016/j. addma.2022.102873
- Lu, Q., Grasso, M., Le, T.-P., and Seita, M. (2022). Predicting build density in L-PBF through *in-situ* analysis of surface topography using powder bed scanner technology. *Addit. Manuf.* 51, 102626. doi:10.1016/j.addma.2022.102626
- Lu, Q. Y., Nguyen, N. V., Hum, A. J. W., Tran, T., and Wong, C. H. (2020). Identification and evaluation of defects in selective laser melted 316L stainless steel parts via *in-situ* monitoring and micro computed tomography. *Addit. Manuf.* 35, 101287. doi:10.1016/j.addma.2020.101287
- Ly, S., Rubenchik, A. M., Khairallah, S. A., Guss, G., and Matthews, M. J. (2017). Metal vapor micro-jet controls material redistribution in laser powder bed fusion additive manufacturing. *Sci. Rep.* 7 (1), 4085–4112. doi:10.1038/s41598-017-04237-z
- Ma, D., Jiang, P., Shu, L., Qiu, Y., Zhang, Y., and Geng, S. (2023). DBN-based online identification of porosity regions during laser welding of aluminum alloys using coherent optical diagnosis. *Opt. Laser Technol.* 165, 109597. doi:10.1016/j.optlastec. 2023.109597
- Matilainen, V.-P., Piili, H., Salminen, A., and Nyrhilä, O. (2015). Preliminary investigation of keyhole phenomena during single layer fabrication in laser additive manufacturing of stainless steel. *Phys. Procedia* 78, 377–387. doi:10.1016/j.phpro. 2015.11.052
- Mi, J., Zhang, Y., Li, H., Shen, S., Yang, Y., Song, C., et al. (2023). *In-situ* monitoring laser based directed energy deposition process with deep convolutional neural network. *J. Intell. Manuf.* 34 (2), 683–693. doi:10.1007/s10845-021-01820-0
- Millon, C., Vanhoye, A., Obaton, A.-F., and Penot, J.-D. (2018). Development of laser ultrasonics inspection for online monitoring of additive manufacturing. *Weld. World* 62 (3), 653–661. doi:10.1007/s40194-018-0567-9
- Min, Y., Shen, S., Li, H., Liu, S., Mi, J., Zhou, J., et al. (2022). Online monitoring of an additive manufacturing environment using a time-of-flight mass spectrometer. *Measurement* 189, 110473. doi:10.1016/j.measurement.2021.110473
- Nakkina, T. G., Vinayaka, M., Masad, A., Mansori, M. E., and Bukkapatnam, S. (2022). Smart defect identification for manufacturing applications. *Surf. Topogr. Metrol. Prop.* 10 (3), 035045. doi:10.1088/2051-672X/ac9247
- Nguyen, T. M., and Wu, Q. M. J. (2013). Fast and robust spatially constrained Gaussian mixture model for image segmentation. *IEEE Trans. Circuits Syst. Video Technol.* 23 (4), 621–635. doi:10.1109/TCSVT.2012.2211176
- O'Dowd, N. M., Wachtor, A. J., and Todd, M. D. (2021). Effects of digital fringe projection operational parameters on detecting powder bed defects in additive manufacturing. *Addit. Manuf.* 48, 102454. doi:10.1016/j.addma.2021.102454
- Özsoy, K., Aksoy, B., and Salman, O. K. M. (2021). Investigation of the dimensional accuracy using image processing techniques in powder bed fusion. *Proc. Institution Mech. Eng. Part E J. Process Mech. Eng.* 235 (5), 1587–1597. doi:10.1177/09544089211011011
- Patel, R., Hirsch, M., Dryburgh, P., Pieris, D., Achamfuo-Yeboah, S., Smith, R., et al. (2018). Imaging material texture of as-deposited selective laser melted parts using spatially resolved acoustic spectroscopy. *Appl. Sci.* 8 (10), 1991. Art. no. 10. doi:10.3390/app8101991
- Pieris, D., Patel, R., Dryburgh, P., Hirsch, M., Li, W., Sharples, S. D., et al. (2019). Spatially resolved acoustic spectroscopy towards online inspection of additive manufacturing. *Insight Non-Destructive Test. Cond. Monit.* 61 (3), 132–137. doi:10. 1784/insi.2019.61.3.132
- Qi, S., Yang, J., and Zhong, Z. (2020). "A review on industrial surface defect detection based on deep learning technology," in presented at the 2020 the 3rd international conference on machine learning and machine intelligence, 24–30.

Radel, S., Diourte, A., Soulié, F., Company, O., and Bordreuil, C. (2019). Skeleton arc additive manufacturing with closed loop control. *Addit. Manuf.* 26, 106–116. doi:10. 1016/j.addma.2019.01.003

- Raffestin, M., Domashenkov, A., Bertrand, P., Faverjon, P., and Courbon, C. (2023). Ultrasonic diagnostic for *in situ* control in metal additive manufacturing. *Measurement* 206, 112244. doi:10.1016/j.measurement.2022.112244
- Regulin, D., and Barucci, R. (2023). A benchmark of approaches for closed loop control of melt pool shape in DED. *Int. J. Adv. Manuf. Technol.* 126 (1–2), 829–843. doi:10.1007/s00170-023-11042-8
- Reich, S., Göbel, A., Goesmann, M., Heunoske, D., Schäffer, S., Lueck, M., et al. (2022). 2D and 3D triangulation are suitable *in situ* measurement tools for high-power large spot laser penetration processes to visualize depressions and protrusions before perforating. *Materials* 15 (11), 3743. Art. no. 11. doi:10.3390/ma15113743
- Renner, J., Breuning, C., Markl, M., and Körner, C. (2022). Surface topographies from electron optical images in electron beam powder bed fusion for process monitoring and control. *Addit. Manuf.* 60, 103172. doi:10.1016/j.addma.2022.103172
- Repossini, G., Laguzza, V., Grasso, M., and Colosimo, B. M. (2017). On the use of spatter signature for *in-situ* monitoring of Laser Powder Bed Fusion. *Addit. Manuf.* 16, 35–48. doi:10.1016/j.addma.2017.05.004
- Sharples, S. D., Clark, M., and Somekh, M. G. (2006). Spatially resolved acoustic spectroscopy for fast noncontact imaging of material microstructure. *Opt. Express, OE* 14 (22), 10435–10440. doi:10.1364/OE.14.010435
- Smith, R. J., Li, W., Coulson, J., Clark, M., Somekh, M. G., and Sharples, S. D. (2014). Spatially resolved acoustic spectroscopy for rapid imaging of material microstructure and grain orientation. *Meas. Sci. Technol.* 25 (5), 055902. doi:10.1088/0957-0233/25/5/055902
- Smoqi, Z., Bevans, B. D., Gaikwad, A., Craig, J., Abul-Haj, A., Roeder, B., et al. (2022). Closed-loop control of meltpool temperature in directed energy deposition. *Mater. Des.* 215, 110508. doi:10.1016/j.matdes.2022.110508
- Sotelo, L. D., Karunakaran, R., Pratt, C. S., Sealy, M. P., and Turner, J. A. (2021). Ultrasound *in situ* characterization of hybrid additively manufactured Ti6Al4V. *J. Acoust. Soc. Am.* 150 (6), 4452–4463. doi:10.1121/10.0008972
- Su, Y., Wang, C., Xu, X., Luo, K., and Lu, J. (2023). Pore defects and corrosion behavior of AISI 316L stainless steel fabricated by laser directed energy deposition under closed-loop control. *Surf. Coatings Technol.* 463, 129527. doi:10.1016/j.surfcoat.2023. 129527
- Su, Y., Wang, Z., Lu, H., Luo, K., and Lu, J. (2022b). Improved wear resistance of directed energy deposited Fe-Ni-Cr alloy via closed-loop controlling laser power. *J. Manuf. Process.* 75, 802–813. doi:10.1016/j.jmapro.2022.01.047
- Su, Y., Wang, Z., Xu, X., Luo, K., and Lu, J. (2022a). Effect of closed-loop controlled melt pool width on microstructure and tensile property for Fe-Ni-Cr alloy in directed energy deposition. *J. Manuf. Process.* 82, 708–721. doi:10.1016/j.jmapro.2022.08.049
- Sun, Z., Guo, W., and Li, L. (2020). In-process measurement of melt pool cross-sectional geometry and grain orientation in a laser directed energy deposition additive manufacturing process. *Opt. Laser Technol.* 129, 106280. doi:10.1016/j.optlastec.2020.
- Tapia, G., and Elwany, A. (2014). A review on process monitoring and control in metal-based additive manufacturing. J. Manuf. Sci. Eng. 136 (6). doi:10.1115/1.4028540
- The global machine vision market (2023). The global machine vision market size was valued at \$9.01 billion in 2022 & is projected to grow from \$9.68 billion in 2023 to \$16.82 billion by 2030.pdf.
- Tiwari, A., Villasenor, E. J., Gupta, N., Reddy, N., Karri, R., and Bukkapatnam, S. T. S. (2021). "Protection against counterfeiting attacks in 3D printing by streaming signature-embedded manufacturing process instructions," in Proceedings of the 2021 Workshop on Additive Manufacturing (3D Printing) Security, in AMSec '21, New York, NY, USA, November 2021 (New York, NY, USA: Association for Computing Machinery), 11–21. doi:10.1145/3462223.3485620
- Vallabh, C. K. P., Xiong, Y., and Zhao, X. (2021). "In-situ monitoring of laser powder bed fusion process anomalies via a comprehensive analysis of off-Axis camera data," in presented at the ASME 2020 15th International Manufacturing Science and Engineering Conference, American Society of Mechanical Engineers Digital Collection. doi:10.1115/MSEC2020-8300
- Wang, K., Dave, P., Hanchate, A., Sagapuram, D., Natarajan, G., and Bukkapatnam, S. T. (2022). Implementing an open-source sensor data ingestion, fusion, and analysis capabilities for smart manufacturing. *Manuf. Lett.* 33, 893–901. doi:10.1016/j.mfglet. 2022.07.109

- Wang, R., Law, A. C., Garcia, D., Yang, S., and Kong, Z. (2021). Development of structured light 3D-scanner with high spatial resolution and its applications for additive manufacturing quality assurance. *Int. J. Adv. Manuf. Technol.* 117 (3), 845–862. doi:10. 1007/s00170-021-07780-2
- Wang, Z., Liu, R., Sparks, T., Liu, H., and Liou, F. (2015). Stereo vision based hybrid manufacturing process for precision metal parts. *Precis. Eng.* 42, 1–5. doi:10.1016/j. precisioneng.2014.11.012
- Wolff, S. J., Wang, H., Gould, B., Parab, N., Wu, Z., Zhao, C., et al. (2021b). *In situ* X-ray imaging of pore formation mechanisms and dynamics in laser powder-blown directed energy deposition additive manufacturing. *Int. J. Mach. Tools Manuf.* 166, 103743. doi:10.1016/j.ijmachtools.2021.103743
- Wolff, S. J., Webster, S., Parab, N. D., Aronson, B., Gould, B., Greco, A., et al. (2021a). *In-situ* observations of directed energy deposition additive manufacturing using high-speed X-ray imaging. *JOM* 73 (1), 189–200. doi:10.1007/s11837-020-04469-x
- Wong, H. (2020). Pilot investigation of surface-tilt and gas amplification induced contrast during electronic imaging for potential *in-situ* electron beam melting monitoring. *Addit. Manuf.* 35, 101325. doi:10.1016/j.addma.2020.101325
- Wong, H., Neary, D., Shahzad, S., Jones, E., Fox, P., and Sutcliffe, C. (2019). Pilot investigation of feedback electronic image generation in electron beam melting and its potential for in-process monitoring. *J. Mater. Process. Technol.* 266, 502–517. doi:10. 1016/j.jmatprotec.2018.10.016
- Xie, J., Jiang, T., and Chen, X. (2022). An image segmentation framework for *in-situ* monitoring in laser powder bed fusion additive manufacturing. *IFAC-PapersOnLine* 55 (37), 800–806. doi:10.1016/j.ifacol.2022.11.280
- Xiong, J., Yin, Z., and Zhang, W. (2016). Closed-loop control of variable layer width for thin-walled parts in wire and arc additive manufacturing. *J. Mater. Process. Technol.* 233, 100–106. doi:10.1016/j.jmatprotec.2016.02.021
- Yan, H., Grasso, M., Paynabar, K., and Colosimo, B. M. (2022). Real-time detection of clustered events in video-imaging data with applications to additive manufacturing. *IISE Trans.* 54 (5), 1–28. doi:10.1080/24725854.2021.1882013
- Yang, H.-C., Huang, C.-H., Adnan, M., Hsu, C.-H., Lin, C.-H., and Cheng, F.-T. (2021). An online AM quality estimation architecture from pool to layer. *IEEE Trans. Autom. Sci. Eng.* 18 (1), 269–281. doi:10.1109/TASE.2020.3012622
- Yang, Z., Zhu, L., Dun, Y., Ning, J., Wang, S., Xue, P., et al. (2023). *In-situ* monitoring of the melt pool dynamics in ultrasound-assisted metal 3D printing using machine learning. *Virtual Phys. Prototyp.* 18 (1), e2251453. doi:10.1080/17452759.2023.2251453
- Yoshizawa, T. (2009). Handbook of optical metrology: principles and applications. CRC Press.
- You, D., Gao, X., and Katayama, S. (2014). WPD-PCA-based laser welding process monitoring and defects diagnosis by using FNN and SVM. *IEEE Trans. Industrial Electron.* 62 (1), 628–636. doi:10.1109/tie.2014.2319216
- Zhang, B., Ziegert, J., Farahi, F., and Davies, A. (2016). *In situ* surface topography of laser powder bed fusion using fringe projection. *Addit. Manuf.* 12, 100–107. doi:10. 1016/j.addma.2016.08.001
- Zhang, W., Wang, J., Tang, M., Ma, H., Wang, L., Zhang, Q., et al. (2023b). 2-D transformer-based approach for process monitoring of metal 3-D printing via coaxial high-speed imaging. *IEEE Trans. Industrial Inf.*, 1–11. doi:10.1109/TII. 2023.3314071
- Zhang, X., Shen, W., Suresh, V., Hamilton, J., Yeh, L. H., Jiang, X., et al. (2021). *In situ* monitoring of direct energy deposition via structured light system and its application in remanufacturing industry. *Int. J. Adv. Manuf. Technol.* 116 (3), 959–974. doi:10.1007/s00170-021-07495-4
- Zhang, X., Zheng, Y., Suresh, V., Wang, S., Li, B., et al. (2020). Correlation approach for quality assurance of additive manufactured parts based on optical metrology. *J. Manuf. Process.* 53, 310–317. doi:10.1016/j.jmapro.2020.02.037
- Zhang, Y., Zhang, P., Jiang, X., Zhang, S., Zhong, K., and Li, Z. (2023a). *In-situ* 3D contour measurement for laser powder bed fusion based on phase guidance. *Theor. Appl. Mech. Lett.* 13 (2), 100405. doi:10.1016/j.taml.2022.100405
- Zhao, C., Fezzaa, K., Cunningham, R. W., Wen, H., De Carlo, F., Chen, L., et al. (2017). Real-time monitoring of laser powder bed fusion process using high-speed X-ray imaging and diffraction. *Sci. Rep.* 7 (1), 3602. Art. no. 1. doi:10.1038/s41598-017-03761-2
- Zhong, R. Y., Xu, X., Klotz, E., and Newman, S. T. (2017). Intelligent manufacturing in the context of industry 4.0: a review. *Engineering* 3 (5), 616–630. doi:10.1016/j.eng. 2017.05.015